

Electronic Supplementary Information

Facile and scalable synthesis of topologically nanoengineered polypeptides with excellent antimicrobial activities

Yu Zhang,^a Wenliang Song,^a Shuwei Li,^b Dae-Kyoung Kim,^c Jae Ho Kim,^c Jung Rae Kim,^b Il Kim^{*a}

^aBK21 PLUS Center for Advanced Chemical Technology, Department of Polymer Science and Engineering, Pusan National University, Busan 609-735, Republic of Korea. E-mail:

ilkim@pusan.ac.kr

^bSchool of Chemical and Biomolecular Engineering, Pusan National University, Busan, 46241, Republic of Korea.

^cDepartment of Physiology, School of Medicine, Pusan National University, Yangsan 626-870, Gyeongsangnam-do, Republic of Korea.

1. Materials and instrumentation

Materials. Anhydrous *N,N*-dimethylformamide (DMF) and trifluoroacetic acid (TFA) were purchased from Alfa Aesar and used without further purification. Tetrahydrofuran (THF), diethyl ether, hexane, ethyl acetate, and methanol were purchased from Alfa Aesar and purified by treatment with calcium disulfide under N₂. *L*-Glutamic acid 5-benzyl ester (H-Glu(OBn)-OH), *Nε-tert*-butyloxycarbonyl-*L*-lysine (H-Lys(Boc)-OH), and 1,3-diisopropylimidazolium chloride were purchased from Alfa Aesar and stored under N₂. Aniline (ANI), ethylenediamine (EDA), and tris-(2-aminoethyl)amine (TREN) were purchased from Sigma-Aldrich and used as received. Other chemicals (MgSO₄, KHCO₃ and triphosgene) were purchased from Alfa Aesar and used as received. Deuterated solvents were purchased from BK Instruments, Inc. and used without further purification. All reactions and polymerizations were performed in a glove box or with Schlenk techniques under N₂. *Escherichia coli* BL21 (*E. coli*) and *Bacillus subtilis* ATCC 6633 (*B. subtilis*) were provided by Korean Collection for Type Cultures.

Instrumentation. ^1H and ^{13}C nuclear magnetic resonance (NMR) spectra were recorded on a Varian Unity 400 MHz spectrometer with shifts reported in parts per million downfield from tetramethylsilane and referenced to the residual solvent peak.

Size exclusion chromatography (SEC) analyses were performed by using a Wyatt system equipped with PL gel (5 μm), mixed-c 750 \times 300 mm columns, a Wyatt DAWN HELEOS-II multi-angle light scattering detector, and Wyatt Optilab rEX differential refractive index detector with a 658-nm light source. The column temperature and the detector temperature were kept at 45 $^\circ\text{C}$. DMF containing 0.1 M LiBr was used as the eluent at a flow rate of 0.5 $\text{mL}\cdot\text{min}^{-1}$. The molecular weights (M_n) and dispersity (D) of the resultant polymers were determined with RI and a calibration curve that was constructed using polystyrene standards. All data analyses were performed using Wyatt Astra V 6.1.1 software.

Fourier Transform infrared (FT-IR) spectroscopic data were collected for film samples cast on a KBr disk, which was determined using a Shimadzu IRPrestige-21 spectrophotometer with 32 scans per experiment at a resolution of 1 cm^{-1} .

Matrix-assisted laser desorption/ionization-time of flight (MALDI-TOF) mass spectra were acquired at the Materials Characterization Lab using a MALDI TOF-TOF 5800 System (AB SCIEX, USA) equipped with a N_2 laser emitting at 337 nm with a 3-ns pulse duration. The instrument was operated in reflector mode and the ions were accelerated under a potential of 20 kV. Potassium/sodium trifluoroacetates were added as a cation source and 2,5-dihydroxybenzoic acid were used as matrices. All samples were dissolved in chloroform/TFA (1:1) at a concentration of 2 $\text{mg}\cdot\text{mL}^{-1}$ and samples for MALDI-TOF MS were prepared by mixing the polymer, matrix, and a cationization agent.

Dynamic light scattering (DLS) and zeta potential measurements were performed on a Malvern Zetasizer Nano ZS apparatus equipped with a monochromatic coherent He-Ne laser (633 nm) as the light source and a detector to detect scattered light at an angle of 173 $^\circ$ and a constant temperature of 25 $^\circ\text{C}$. Measurements were performed at concentrations of 2 $\text{mg}\cdot\text{mL}^{-1}$ in Milli Q water. All samples filtered through 0.45 μm nylon filters prior to measurement and were performed in triplicate.

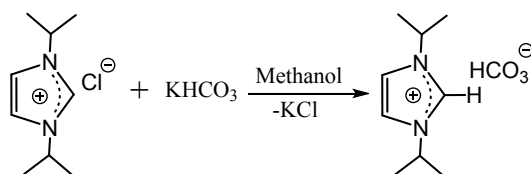
UV-vis spectroscopy analysis was performed using a Shimadzu UV-1650 PC with a scan speed of 300 nm·min⁻¹. The absorbance and transmittance spectra of the TNAPs/bacteria mixed solution were recorded at 600 nm.

Circular Dichroism (CD) analyses were performed in a JASCO J-1500 spectrometer with a 0.1 nm quartz cells at 25 °C. The TNAPs were dissolved in Milli-Q water to 0.5 mg·mL⁻¹. Wavelengths between 190 and 260 nm were analyzed, with an integration time of 1 s and a wavelength step of 0.2 nm. The Milli-Q water was used as the reference solvent and five scans were recorded for all TNAPs.

Scanning electron microscopy (SEM) was applied to detect the cellular morphologies of pathogen. The bacteria were treated with TNAPs at 3 × MIC value and cultivated in a shaking bed at 37 °C for 4 h. And a control was prepared under the same condition without TNAPs added. Both treated group and control group of bacteria were washed three times with phosphate buffered saline (PBS) and the samples fixed with 2.5% (v/v) glutaraldehyde and 4% (v/v) paraformaldehyde in phosphate buffer (0.1 M) for overnight at 4 °C. The fixed bacteria suspension were washed three times with PBS to clear excess fixative, and then transferred to a cover slide and allowed to air-dry. Subsequently, the dried samples were dehydrated in a graded ethanol series (30% – 100%). Finally, both samples were critical point dried and ready for SEM analysis.

2. Experimental procedures and characterization

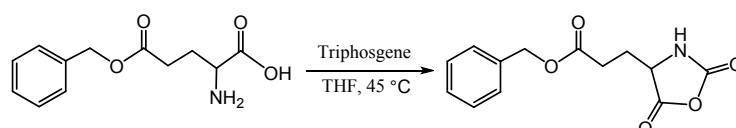
Synthesis of imidazolium hydrogen carbonate (IHC)



IHC Was prepared according to the reported literature procedure.^[S1] 1,3-Diisopropylimidazolium chloride (1 g, 4.28 mmol) was dissolved in 5 mL of methanol. Then 1.2 eq. of dry KHCO₃ was added and the resulting mixture was stirred under a N₂ atmosphere for 48 h at room temperature. The reaction solution was then filtered to remove KCl and the filtrate was evaporated under vacuum to remove the remaining

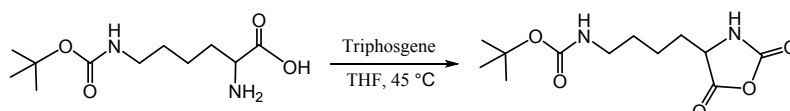
methanol. The crude product was washed several times with acetone and dried under vacuum. Yield: 79.3%. ^1H NMR (MeOD, 400 MHz): δ 1.62 (d, 12H, CH_3iPr), 4.73 (sept, 2H, $\text{CH}i\text{Pr}$), 7.78 (s, 2H, $-\text{CH}=\text{CH}-$). The HCO_3^- and N_2CH signals could not be observed due to their rapid exchange with the deuterated solvent on the NMR time-scale. ^{13}C NMR (MeOD, 100 MHz): δ 23.2, 54.9, 122.0, 134.5, 161.6.

Synthesis of (*S*)- γ -benzyl-*L*-glutamate-*N*-carboxyanhydride (BLG NCA)



BLG NCA was synthesized by following the previously reported procedure.^[S2,S3] H-Glu(OBn)-OH (3.56 g, 15 mmol) suspended in 50 mL of anhydrous THF was fed into a Schlenk flask fitted with a N_2 atmosphere and a rubber septum at 45 °C. 0.5 eq. Of triphosgene dissolved in THF was then slowly added. After the mixture turned clear and no particles remained at the bottom of the flask, the solution was cooled to room temperature and bubbled with N_2 to remove unreacted phosgene and HCl, and concentrated in vacuo. The crude product was finally recrystallized thrice by the addition of excess hexane and THF and dried under vacuum to afford white crystals. Yield: 2.84 g, 71.3%. ^1H NMR ($\text{DMSO}-d_6$, 400 MHz): δ 1.93 (m, 1H, γ -CH), 2.03 (m, 1H, γ -CH), 2.54 (t, 2H, β - CH_2), 4.51 (dd, 1H, α -CH), 5.11 (s, 2H, $-\text{CH}_2\text{Ar}$), 7.36 (m, 5H, ArH), 9.11 (s, 1H, $-\text{NH}-$). ^{13}C NMR ($\text{DMSO}-d_6$, 100 MHz): δ 27.2, 29.8, 57.1, 57.2, 128.8, 128.9, 129.3, 136.8, 152.4, 172.1, 174.3.

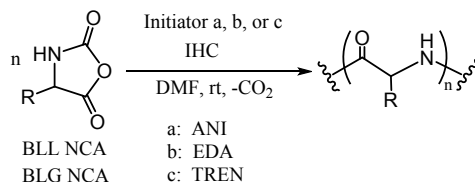
Synthesis of *N* ϵ -tert-butyloxycarbonyl-*L*-lysine-*N*-carboxyanhydride (BLL NCA)



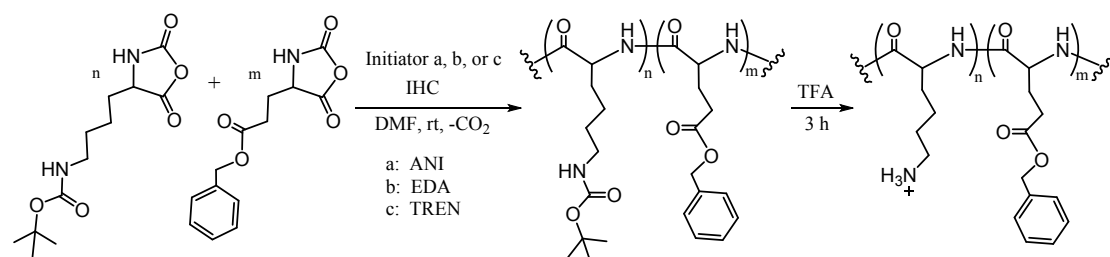
BLL NCA was synthesized by the same procedure used for BLG NCA by employing (H-Lys(Boc)-OH) and triphosgene as the raw materials. Yield: 85.4%. ^1H NMR ($\text{DMSO}-d_6$, 400 MHz): δ 1.32–1.43 (s, 9H, $-\text{C}(\text{CH}_3)_3$), 1.59–1.71 (m, 6H, $-\text{CH}(\text{CH}_2)_3-$), 2.87 (m, 2H, $-\text{NHCH}_2-$), 4.42 (dd, 1H, $-\text{CH}-$), 6.75 (br, 1H, $-\text{NHCH}_2-$), 9.04 (s, 1H, $-\text{NH}-$ ring). ^{13}C NMR ($\text{DMSO}-d_6$, 100 MHz): δ 22.1, 28.7, 29.4, 31.1, 39.8, 57.4, 77.8,

152.4, 156.0, 172.1.

General polymerization procedures



The typical procedure to synthesis poly(butyloxycarbonyl-*L*-lysine) (BocK) and poly(γ -benzyl-*L*-glutamate) (BE) was performed according to the following steps. In a Schlenk flask, 1 mmol of BLG NCA was dissolved in the DMF. Given amount of initiator (ANI, EDA and TREN) was then introduced into the solution and a predetermined amount of IHC/DMF stock solution (500 μ L, 1×10^{-5} mol) was added to the reaction mixture using a syringe. The mixed solution was stirred for a specific time at room temperature and the conversion of BLG NCA was measured by FT-IR spectrum of an aliquot of mixture. The polymerization was quenched by adding 5 mL of diethyl ether after the desired period and an excess amount of diethyl ether was added to further precipitate the quenched mixture. The collected crude product was dissolved in small amount of DMF and precipitated again by adding diethyl ether to the solution. This dissolution-precipitation process was repeated three times to get the purified BEs and then dried under vacuum. A similar procedure was employed for the preparation of the cyclic BEs and BocKs in the absence of amine initiators.



For the preparation of amphiphilic random copolypeptides, poly(butyloxycarbonyl-*L*-lysine)_x-*random*-poly(γ -benzyl-*L*-glutamate)_y (BocK_x-*r*-BE_y), the general procedure is described below. Firstly, 0.5 mmol of BLG NCA and 0.5 mmol of BLL NCA were dissolved in the DMF. Given amount of initiator (ANI, EDA and TREN) and a

predetermined amount of IHC/DMF stock solution (500 μL , 1×10^{-5} mol) were then added to the monomer solution, respectively. The reaction mixture was stirred for 1–2 h at room temperature until the complete conversion of NCA, as measured by FT-IR spectrum of an aliquot of mixture. An excess amount of diethyl ether was then added to precipitate the reaction mixture. The collected crude BocK_x-*r*-BE_y was treated by dissolution-precipitation process for three times and then dried under vacuum for the further deprotection step. The cyclic BocK_x-*r*-BE_y was synthesized by the similar procedure in the absence of amine initiators.

Acid hydrolysis process was performed to access TNAPs. Neat TFA (2 mL) was added to a Schlenk flask containing the resultant BocK_x or BocK_x-*r*-BE_y, and the mixture was stirred for 3 h at room temperature. The reaction mixture was concentrated to 0.5 mL and then dissolved in 0.5 mL methanol followed by addition of excess amount of diethyl ether to precipitate out the deprotected polymers. The crude product was obtained after three cycles of dissolution/precipitation process, and the collected polymer was dissolved in milli-Q water and then subjected to lyophilization. The final K_x or K_x-*r*-BE_y were obtained as a fluffy white solid and used for further antibacterial activity studies.

Antimicrobial Assay

E. coli and *B. subtilis* cells were cultivated overnight in LB broth medium at 37 °C. The sterilized LB broth (50 mL) was added in the sterilized culture dish. Broth containing bacteria were added into the above-mentioned sterilized LB broth and mixed up evenly to afford the diluted broth-containing bacteria suspension with a concentration of 5×10^7 CFU·mL⁻¹. 3.6 mL of the diluted broth-containing bacteria suspension was added to several 5 mL of sterilized quartz cuvettes. Stock solutions of the TNAPs were prepared in milli-Q water at a concentration of 5.12 mg·mL⁻¹, and then serially diluted to several stock solutions. Each stock solution (400 μL) was added to each quartz cuvette to obtain the mixture of bacteria and TNAPs. 400 μL Of milli-Q water was added to 3.6 mL of diluted broth-containing bacteria suspension, which was set as the control. The bacteria in the cuvettes were cultivated overnight in the shaking bed at 80

rpm and 37 °C. The OD values of bacteria suspension were measured at 600 nm wavelength every 3 h using the UV–vis spectroscopy. The MIC value is defined as the minimum concentration of the sample to inhibit bacterial growth in the cuvettes. All assays were performed in triplicate on different days.

LIVE/DEAD® Baclight™ bacterial viability kit reagents were used to staining bacteria. Syto9 dye binds the viable bacterial cells having an intact membrane, forming a green fluorescence, whereas propidium iodide can traverse the damaged bacteria membrane and interact with DNA giving a red fluorescence. The cultivated *E. coli* and *B. subtilis* were treated with TNAPs at $3 \times \text{MIC}$ value and were washed twice with PBS. Both control and treated groups of bacteria were incubated with propidium iodide and SYTO9 ($10 \mu\text{g}\cdot\text{mL}^{-1}$ final concentration) for 15 min in dark at 37 °C. The strains were then washed twice and resuspended in PBS, 40 μL aliquot of the control and treated bacteria suspensions were added onto glass slides and enclosed by glass coverslip slides. The images were captured using a confocal laser-scanning microscope (ZEISS LSM 800).

Cytotoxicity Assay

The cytotoxicity of as-obtained polymers was evaluated by using MTT assay. The mouse embryonic fibroblast cell (NIH3T3) were cultured in DMEM medium supplemented with 10% fetal bovine serum FBS0 and $100 \text{ IU}\cdot\text{mL}^{-1}$ antibiotics at 37 °C and 5% CO_2 atmosphere. The cells were resuspended in fresh DMEM medium, and 100 μL of the suspension containing 1×10^5 cell/mL was seeded in each well of a 96-well plate for 24 h at 37 °C. Thereafter, the medium was replaced with 100 μL of the prepared polymer solutions and was incubated for 24 h at 37 °C. The control group was carried out using fresh DMEM medium without polymer. After incubation, 100 μL of MTT solution ($0.5 \text{ mg}\cdot\text{mL}^{-1}$) was added to each well and the plate was incubated at 37 °C for additional 4 h. Then, the supernatant was removed, 100 μL /well of DMSO was added to dissolve the purple formazan crystal under shaking for 15 min. The optical density (OD) values were measured by using a 550 Bio-Rad plate reader and the cell viability of each well was calculated relative to the control well value.

Hemolysis Assay

Hemolytic activity of TNAPs was tested ranging from a concentration of $2 \mu\text{g}\cdot\text{mL}^{-1}$ to $4000 \mu\text{g}\cdot\text{mL}^{-1}$. Fresh mice blood was washed three times with PBS and was then diluted to 10% (v/v) with PBS. An aliquot of $90 \mu\text{L}$ blood was first added into 1.5 mL microfuge tube. Then $10 \mu\text{L}$ of each stock solution of TNAPs was added. The blood suspension was also added to blank PBS as the negative control, and to PBS containing 0.2% Triton-X as the positive control. After incubation at $37 \text{ }^\circ\text{C}$ for 1 h, each mixture was centrifuged at 5000 rpm for 5 min. An aliquot of $70 \mu\text{L}$ supernatant was transferred to each well of a 96-well plate to read the OD values at 350 nm. The percentage of hemolysis relative to TX-100 control was calculated as $[(A_{\text{sample}} - A_{\text{negative}})/(A_{\text{sample}} - A_{\text{positive}})] \times 100\%$, where A_{sample} , A_{negative} and A_{positive} are the OD values of the supernatant from the incubated sample, negative control, and positive control, respectively.

Table S1. Recent development of NCA ring-opening polymerization strategies

Catalysts/Initiators	Metal	Temp.	Time	Polymer topology	Ref.
Imidazolium hydrogen carbonates	No	r.t	10 min–2 h	<i>linear</i> <i>hinged</i> <i>star</i> <i>cyclic</i>	This work
Lithium hexamethyldisilazides	Yes	r.t	10 min–2 h	<i>linear</i>	[S4]
Photoinitiators	No	-	3 h	<i>linear</i>	[S5]
“Allied amines”	No	r.t	1–2 h	<i>linear</i> <i>hinged</i>	[S6]
N ₂ flow	No	r.t	2–19 h	<i>linear</i>	[S7]
Rare earth complexes	Yes	40 °C	24 h	<i>linear</i>	[S8]
Silazane derivatives	No	r.t	24 h	<i>linear</i>	[S9]
Tertiary amine	No	20 °C	4 d	<i>cyclic</i>	[S10]
Imidazole	No	60 °C	2 d	<i>cyclic</i>	[S11]
Transition metal catalysts	Yes	r.t	1 h	<i>linear</i>	[S12]

Table S2. Synthesis and characterization of various TNAPs

TNAPs code	Polymer topology	Initiator	Polymer composition ^a	[BLL NCA] ₀ /[BLG NCA] ₀ /[I] ₀ ^b	M_n (kg·mol ⁻¹)		\bar{D} ^d	D_H ^e (nm)	ζ ^e (mV)
					Calc. ^c	SEC ^d			
<i>l</i> -K ₁ - <i>r</i> -BE ₀	<i>Linear</i>	ANI	ANI-K ₃₅	30:0:1	4.58	4.21	1.25	7.1	35.4
<i>l</i> -K ₁ - <i>r</i> -BE _{0,2}			ANI-K ₂₄ - <i>r</i> -BE ₇	24:6:1	4.70	5.03	1.23	9.4	33.6
<i>l</i> -K ₁ - <i>r</i> -BE ₁			ANI-K ₁₈ - <i>r</i> -BE ₁₇	15:15:1	6.12	5.45	1.32	10.3	26.1
<i>h</i> -K ₁ - <i>r</i> -BE ₀	<i>Hinged</i>	EDA	EDA-K ₆₄	60:0:1	8.26	8.91	1.14	13.2	38.9
<i>h</i> -K ₁ - <i>r</i> -BE _{0,2}			EDA-K ₅₃ - <i>r</i> -BE ₁₅	48:12:1	10.14	9.60	1.05	17.5	35.3
<i>h</i> -K ₁ - <i>r</i> -BE ₁			EDA-K ₃₄ - <i>r</i> -BE ₂₉	30:30:1	10.77	13.04	1.09	20.6	29.7
<i>s</i> -K ₁ - <i>r</i> -BE ₀	<i>Star</i>	TREN	TREN-K ₈₈	90:0:1	11.42	11.71	1.13	19.7	41.5
<i>s</i> -K ₁ - <i>r</i> -BE _{0,2}			TREN-K ₇₈ - <i>r</i> -BE ₁₆	72:18:1	13.65	14.80	1.12	23.5	39.7
<i>s</i> -K ₁ - <i>r</i> -BE ₁			TREN-K ₄₃ - <i>r</i> -BE ₃₉	45:45:1	14.20	15.43	1.17	25.2	34.8
<i>c</i> -K ₁ - <i>r</i> -BE ₀	<i>Cyclic</i>	IHC	IHC-K ₃₃	30:0:1	4.37	4.05	1.19	6.7	34.3
<i>c</i> -K ₁ - <i>r</i> -BE _{0,2}			IHC-K ₂₇ - <i>r</i> -BE ₆	24:6:1	4.92	4.60	1.11	8.0	33.9
<i>c</i> -K ₁ - <i>r</i> -BE ₁			IHC-K ₁₆ - <i>r</i> -BE ₁₉	15:15:1	6.36	7.09	1.15	11.8	25.2

^a Based on Boc-protected polymers. ^b [BLL NCA]₀/[BLG NCA]₀/[I]₀ represents the initial molar ratio of monomer to initiator. ^c Experimental M_n were calculated by ¹H NMR spectrum. ^d Determined by SEC calibrated with polystyrene standards. ^e Hydrodynamic diameters (D_H) and zeta potential (ζ) were determined by DLS.

Table S3. Antimicrobial activity of various TNAPs with different architectures and compositions

TNAPs code	Polymer topology	MIC (μM)	
		<i>E.coli</i>	<i>B.subtilis</i>
<i>l</i> -K ₁ - <i>r</i> -BE ₀	<i>Linear</i>	3.41	5.24
<i>l</i> -K ₁ - <i>r</i> -BE _{0.2}		1.70	3.40
<i>l</i> -K ₁ - <i>r</i> -BE ₁		5.22	7.83
<i>h</i> -K ₁ - <i>r</i> -BE ₀	<i>Hinged</i>	2.87	3.87
<i>h</i> -K ₁ - <i>r</i> -BE _{0.2}		1.58	2.36
<i>h</i> -K ₁ - <i>r</i> -BE ₁		3.71	5.94
<i>s</i> -K ₁ - <i>r</i> -BE ₀	<i>Cyclic</i>	2.11	2.80
<i>s</i> -K ₁ - <i>r</i> -BE _{0.2}		1.17	1.75
<i>s</i> -K ₁ - <i>r</i> -BE ₁		2.89	4.51
<i>c</i> -K ₁ - <i>r</i> -BE ₀	<i>Star</i>	3.65	3.65
<i>c</i> -K ₁ - <i>r</i> -BE _{0.2}		1.62	3.23
<i>c</i> -K ₁ - <i>r</i> -BE ₁		5.02	6.29

Table S4. Minimum inhibition concentrations of antimicrobial TNAPs bearing lysine groups

Sample code	MIC (μM)		Ref.
	<i>E. coli</i>	<i>B. subtilis</i>	
<i>s</i> -K ₁ - <i>r</i> -BE _{0.2}	1.15	1.75	This work
P(ManEMA) ₁₀ -p(Lys) ₂₀ ^a	1.6	—	[S13]
PCL ₄₇ - <i>b</i> -p(Lys ₃₈ - <i>stat</i> -Phe ₂₀) ^b	2.42	—	[S14]
C ₁₈ K ₅ ^c	1.08	—	[S15]
PCL ₁₆ - <i>b</i> -K ₂₀ ^d	1.42	—	[S16]
PLLA ₃₁ - <i>b</i> -p(Phe ₂₄ - <i>stat</i> -Lys ₃₆) ^e	3.83	—	[S17]
S16 _L ^f	0.085	—	[S18]
PMACs ^g	2.9	—	[S19]
pLys- <i>r</i> -PBLG ^h	1.94	0.48	[S4]
E18a c(kVOrnLfFYOrnLq) ⁱ	12.62	25.24	[S20]

^aPoly(mannosyloxy ethyl methacrylate)₁₀-poly(lysine)₂₀; ^bPoly(ϵ -caprolactone)₄₇-*block*-poly(lysine₃₈-*stat*-phenylalanine₂₀); ^cC₁₈K₅ was synthesized by standard Fmoc solid-phase peptide synthesis using rink amide resin; ^dPoly(ϵ -caprolactone)₁₆-*block*-poly(lysine)₂₀; ^ePoly(*L*-lactide)-*block*-poly(phenylalanine₂₄-*stat*-lysine₃₆); ^fPoly(amido amine)-poly(lysine-*random*-valine); ^gPeptide-mimetic alternating copolymers; ^hPoly(Lysine)_{0.5}-*random*-poly(γ -benzyl-*L*-glutamate)_{0.5}; ⁱCyclic peptide was synthesized by standard Fmoc solid-phase peptide synthesis.

Table S5. Hemolytic activity and therapeutic index of various TNAPs against fresh red blood cells of mice

TNAPs code	Polymer topology	Mass fraction of lysine units (%) ^a	HC ₅₀ (μg·mL ⁻¹) ^b	Therapeutic index ^c	
				<i>E.coli</i>	<i>B.subtilis</i>
<i>l</i> -K ₁ - <i>r</i> -BE ₀		100	> 4000	> 165	> 125
<i>l</i> -K ₁ - <i>r</i> -BE _{0.2}	<i>Linear</i>	73	> 4000	> 250	> 165
<i>l</i> -K ₁ - <i>r</i> -BE ₁		39	> 4000	> 100	> 60
<i>h</i> -K ₁ - <i>r</i> -BE ₀		100	> 4000	> 165	> 125
<i>h</i> -K ₁ - <i>r</i> -BE _{0.2}	<i>Hinged</i>	67	> 4000	> 250	> 165
<i>h</i> -K ₁ - <i>r</i> -BE ₁		40	> 4000	> 100	> 60
<i>s</i> -K ₁ - <i>r</i> -BE ₀		100	> 4000	> 250	> 165
<i>s</i> -K ₁ - <i>r</i> -BE _{0.2}	<i>Cyclic</i>	65	> 4000	> 500	> 250
<i>s</i> -K ₁ - <i>r</i> -BE ₁		37	> 4000	> 125	> 80
<i>c</i> -K ₁ - <i>r</i> -BE ₀		100	> 4000	> 250	> 250
<i>c</i> -K ₁ - <i>r</i> -BE _{0.2}	<i>Star</i>	70	> 4000	> 500	> 250
<i>c</i> -K ₁ - <i>r</i> -BE ₁		34	> 4000	> 125	> 100

^a Mass fraction of lysine units values were derived from ¹H NMR spectra. ^b HC₅₀ is defined as the minimum polymer concentration that produces 50% hemolysis compared to the positive control treated with 0.2% Triton X-100. All HC₅₀ values of TNAPs were larger than 4000 μg·mL⁻¹. ^c Therapeutic index was calculated as HC₅₀/MIC.

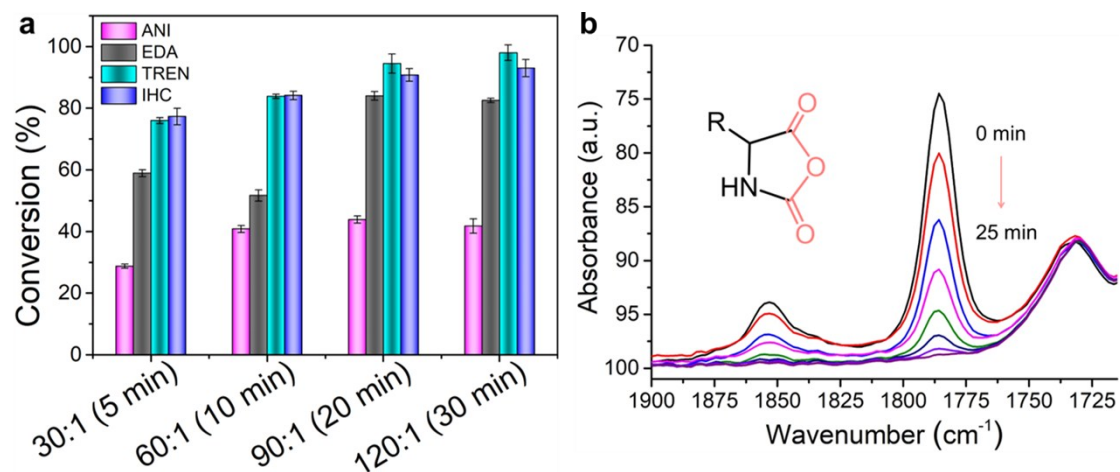


Fig. S1 (a) Conversion of BLG NCA in IHC-organocatalyzed polymerization at variable $[M]_0/[I]_0$ ratios. (b) FT-IR spectrum shows IHC-organocatalyzed polymerization of BLG NCAs in the presence of TREN.

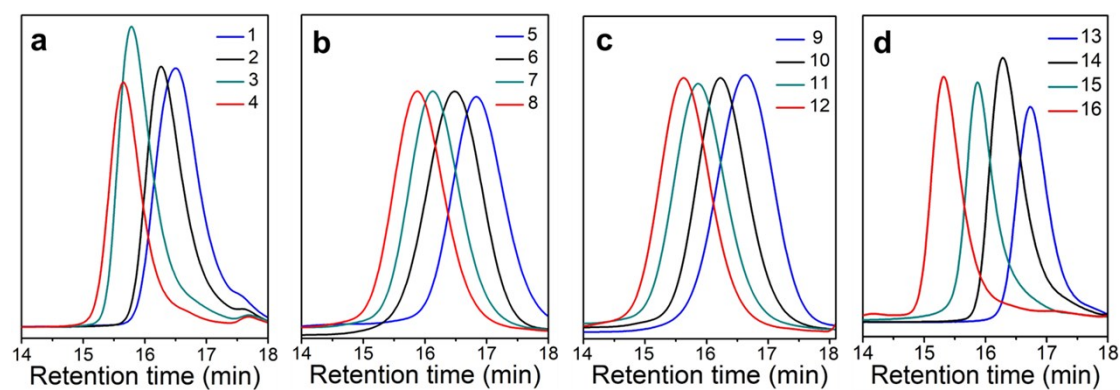


Fig. S2 SEC traces of resultant BEs corresponding to entries 1–16 in Table 1.

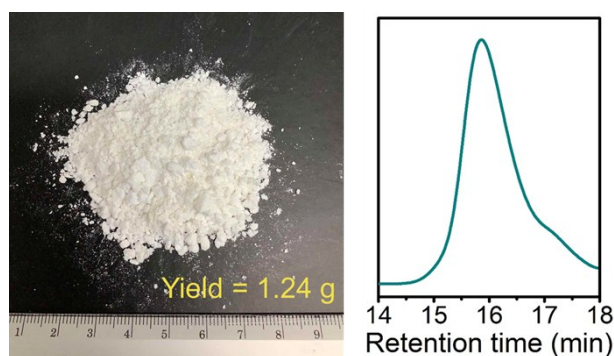


Fig. S3 Photograph and corresponding SEC trace of resulting *star*-BE from gram-scale synthesis ($M_n = 21.43 \text{ kg} \cdot \text{mol}^{-1}$, $D = 1.27$).

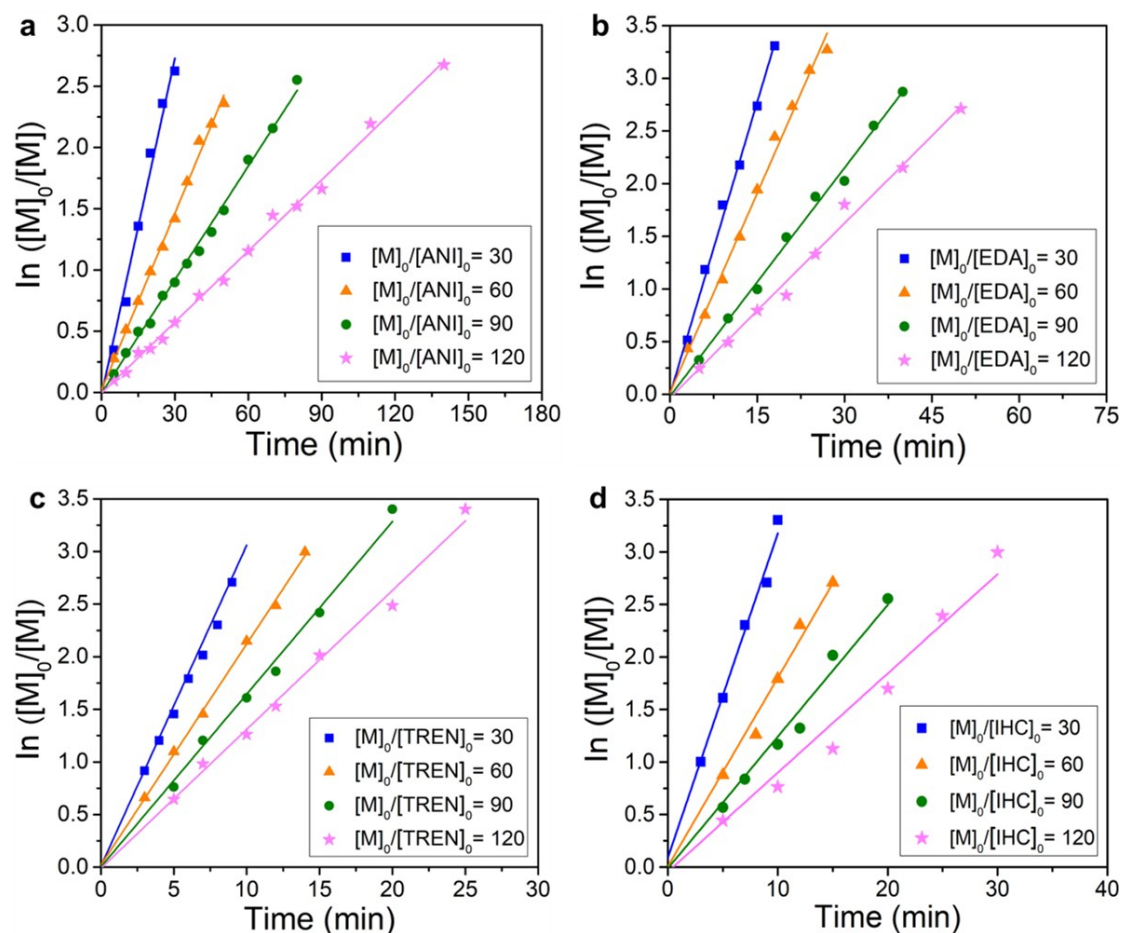


Fig. S4 Plots of $\ln ([M]_0/[M])$ versus time of IHC-catalyzed polymerizations of BLG NCA at variable $[M]_0/[I]_0$ ratios ($[M]_0 = 0.2$ M) in the presence of ANI, EDA and TREN initiators and in the absence of amine initiators.

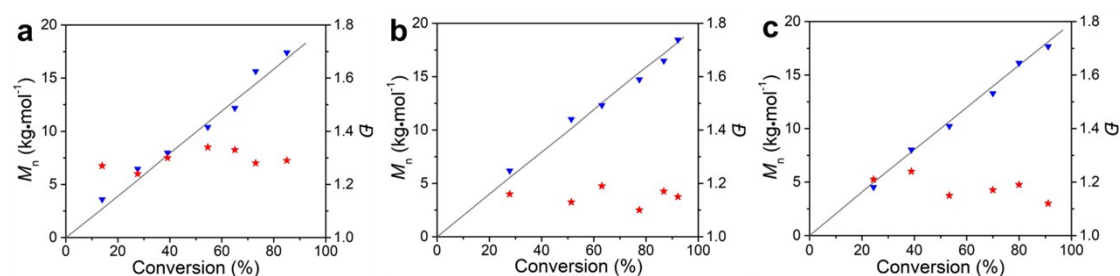


Fig. S5 Plots of M_n and \bar{D} versus monomer conversion for IHC-mediated polymerization of BLG NCA in the presence of (a) ANI, (b) EDA, and (c) TREN initiators with $[M]_0/[I]_0/[IHC]_0 = 90:1:0.3$ and $[M]_0 = 0.2$ M. The M_n values of the resultant BE increase linearly with the conversion of BLG NCA, corroborating a constant concentration of propagation chains throughout the course of the polymerization.

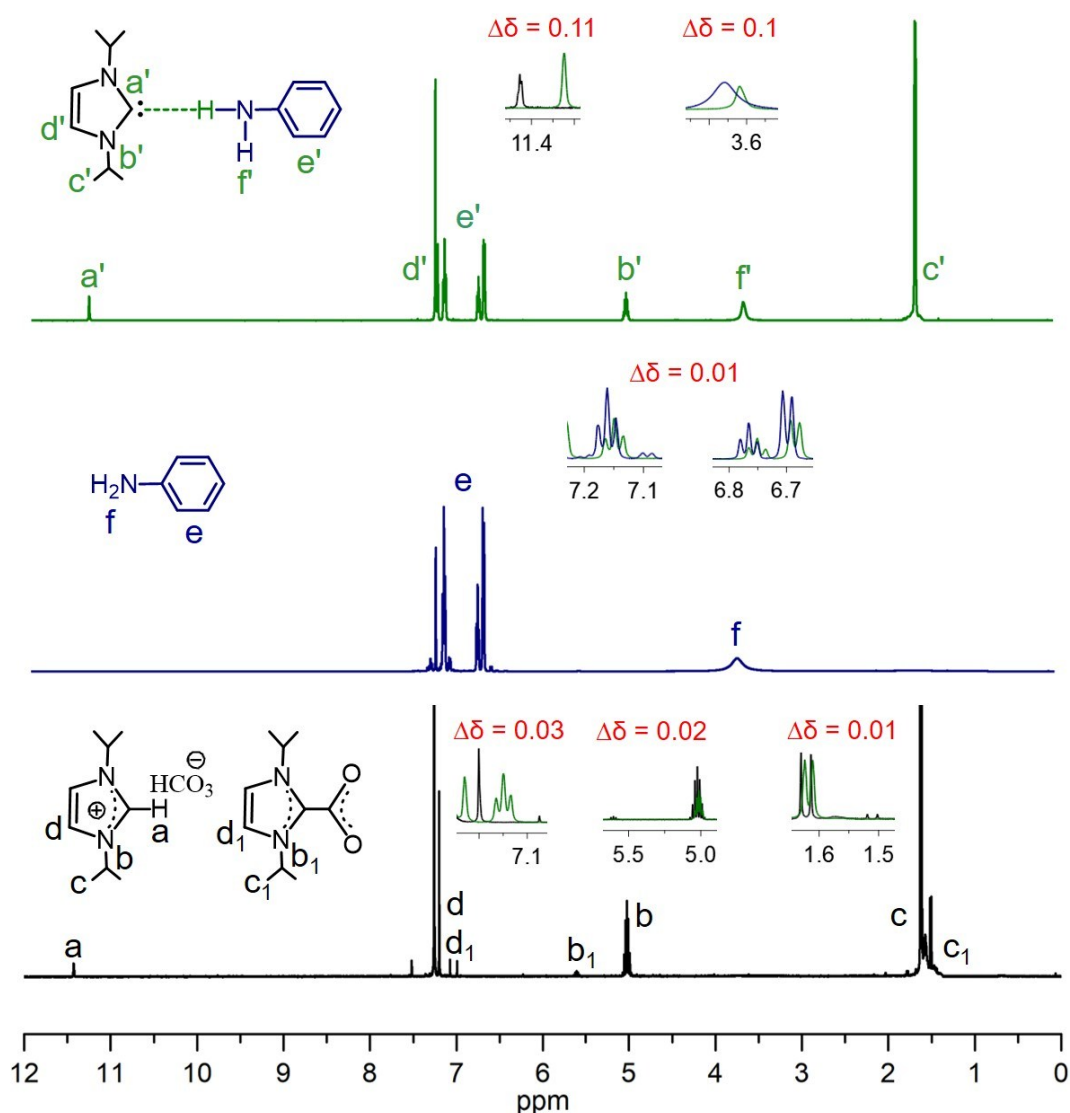


Fig. S6 ¹H NMR spectra of IHC (black), ANI (blue), and an equimolar mixture of IHC and ANI (green) in CDCl₃. (To understand the high activity of amine-induced polymerization in the presence of IHC, we investigated the interaction between amine and IHC by utilizing ¹H NMR spectroscopy (Fig. S6–S8). The ¹H NMR comparative study of IHC, amine and IHC/amine mixture revealed the relatively larger chemical shift of N-H protons in amines followed by the slightly chemical shift of other C-H protons in IHC and amines, suggesting the non-covalent interaction between amine and IHC most likely to be hydrogen-bonding interaction. This hydrogen-bonding interaction will enhance the activity of amines and promoting the following nucleophilic attack on NCAs).

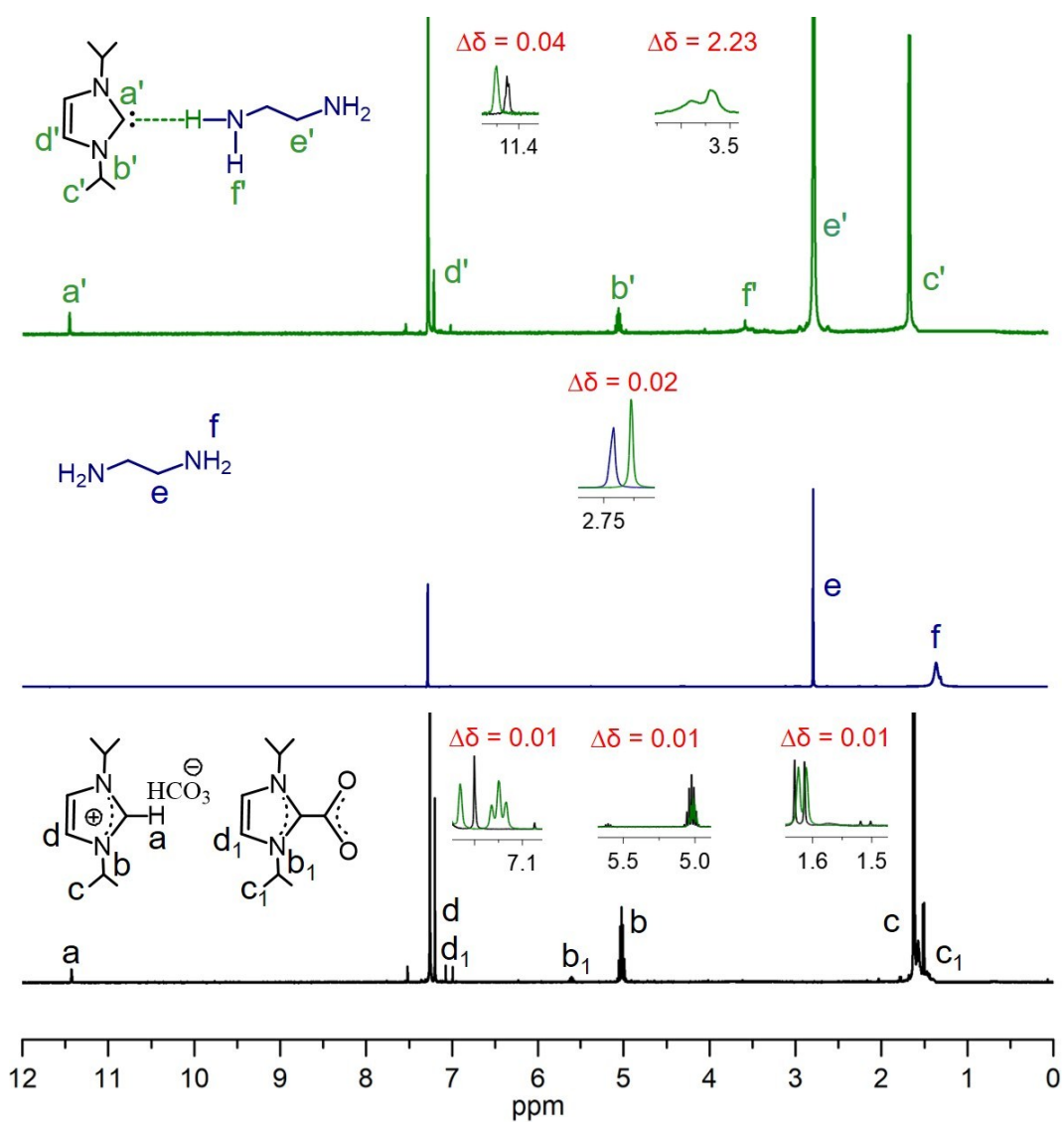


Fig. S7 ^1H NMR spectra of IHC (black), EDA (blue), and an equimolar mixture of IHC and EDA (green) in CDCl_3 .

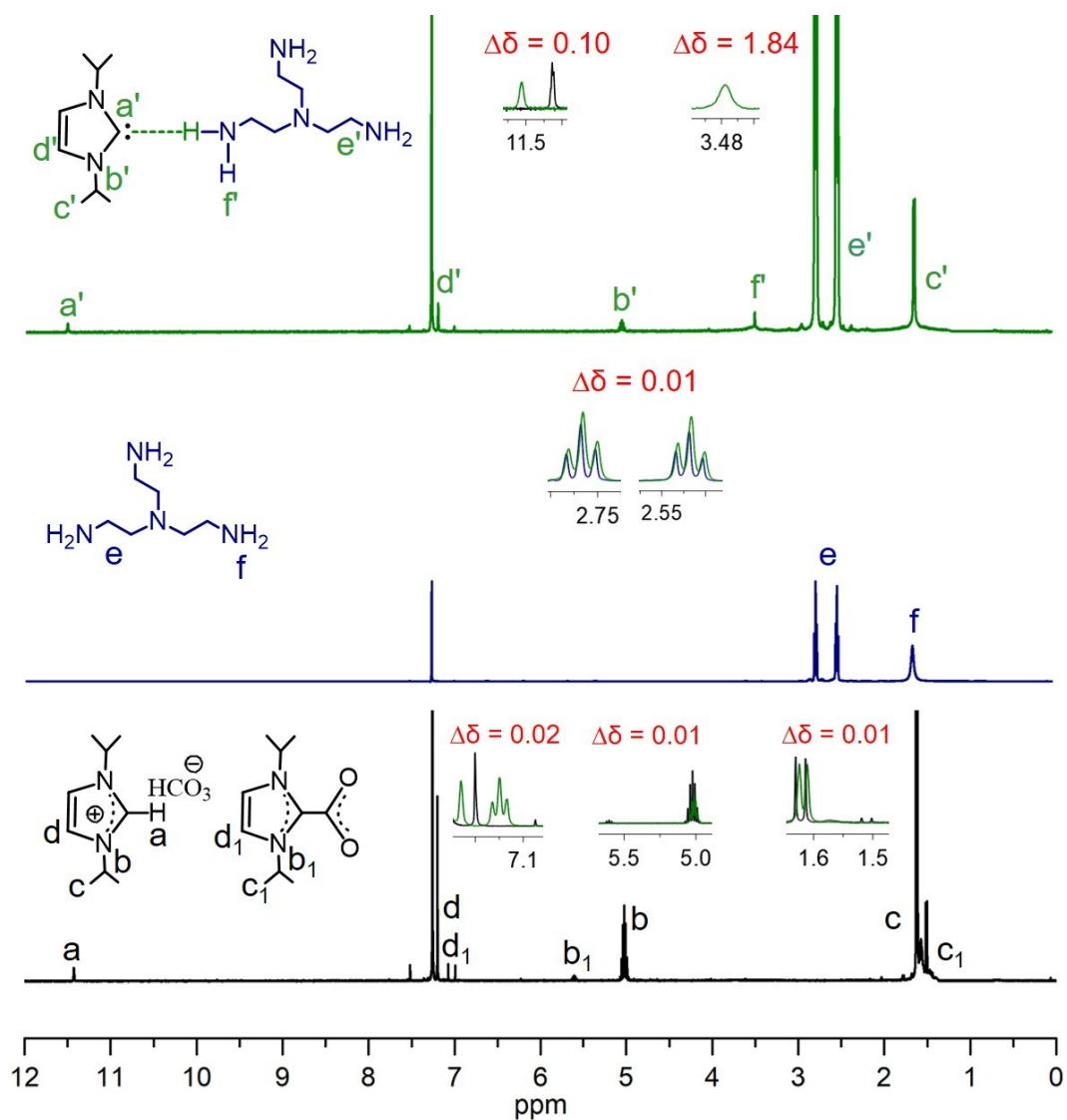


Fig. S8 ¹H NMR spectra of IHC (black), TREN (blue), and an equimolar mixture of IHC and TREN (green) in CDCl₃.

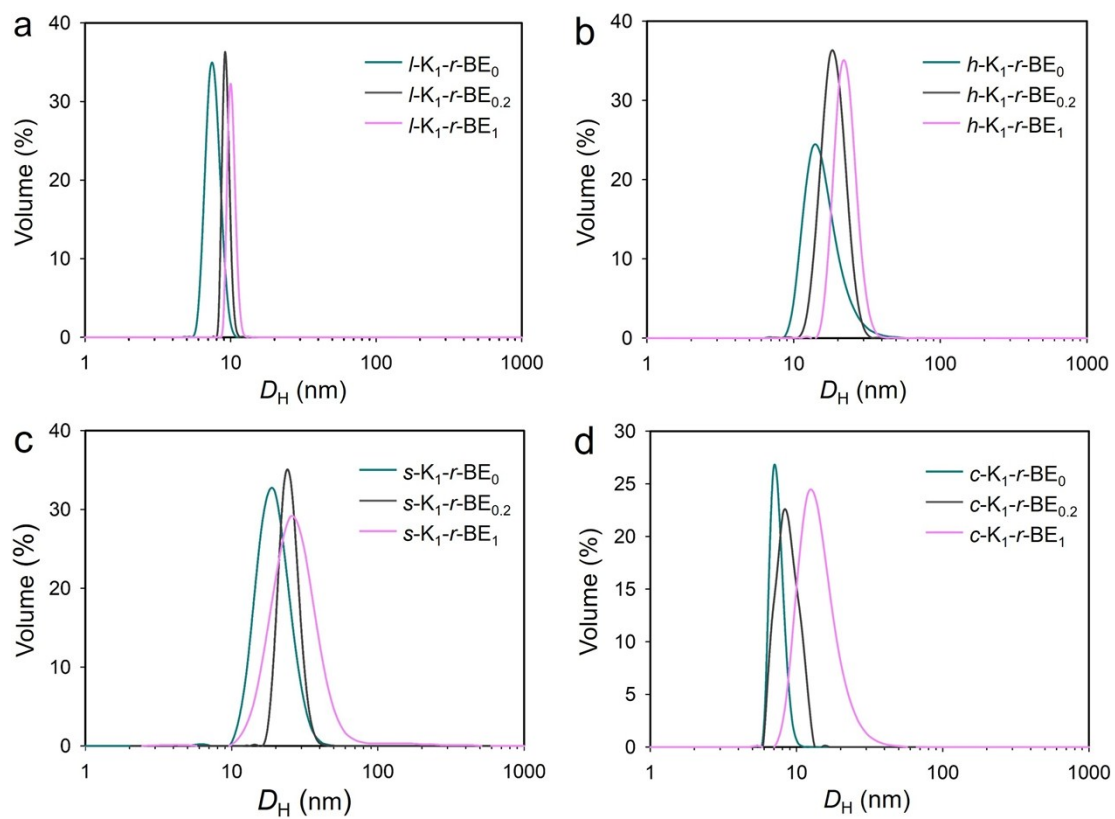


Fig. S9 DLS traces of TNAPs. Measurements were performed at concentrations of $2 \text{ mg}\cdot\text{mL}^{-1}$ in Milli-Q water.

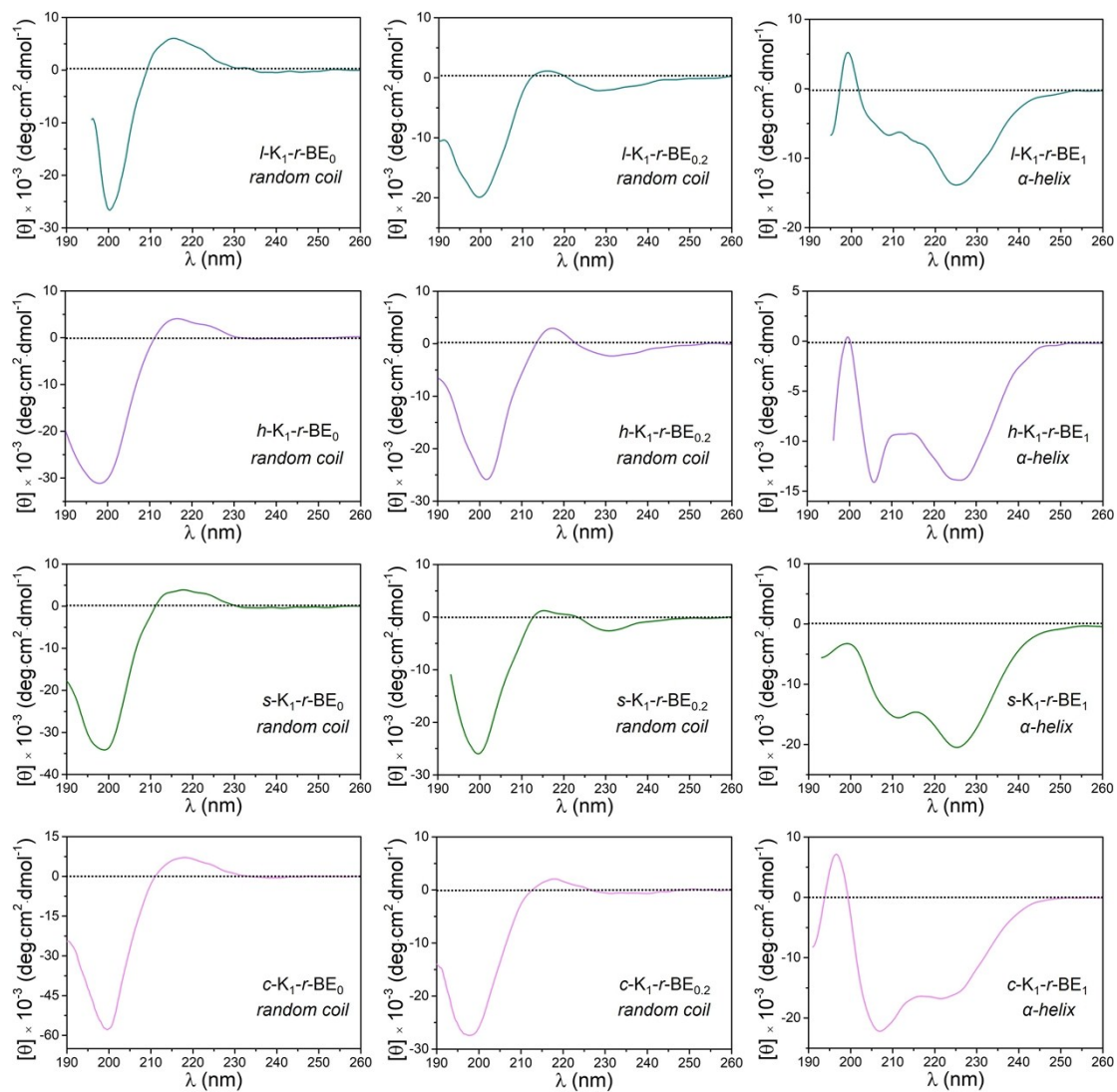


Fig. S10 CD spectra of the TNAPs with a concentration of $0.5 \text{ mg}\cdot\text{mL}^{-1}$ in Milli-Q water.

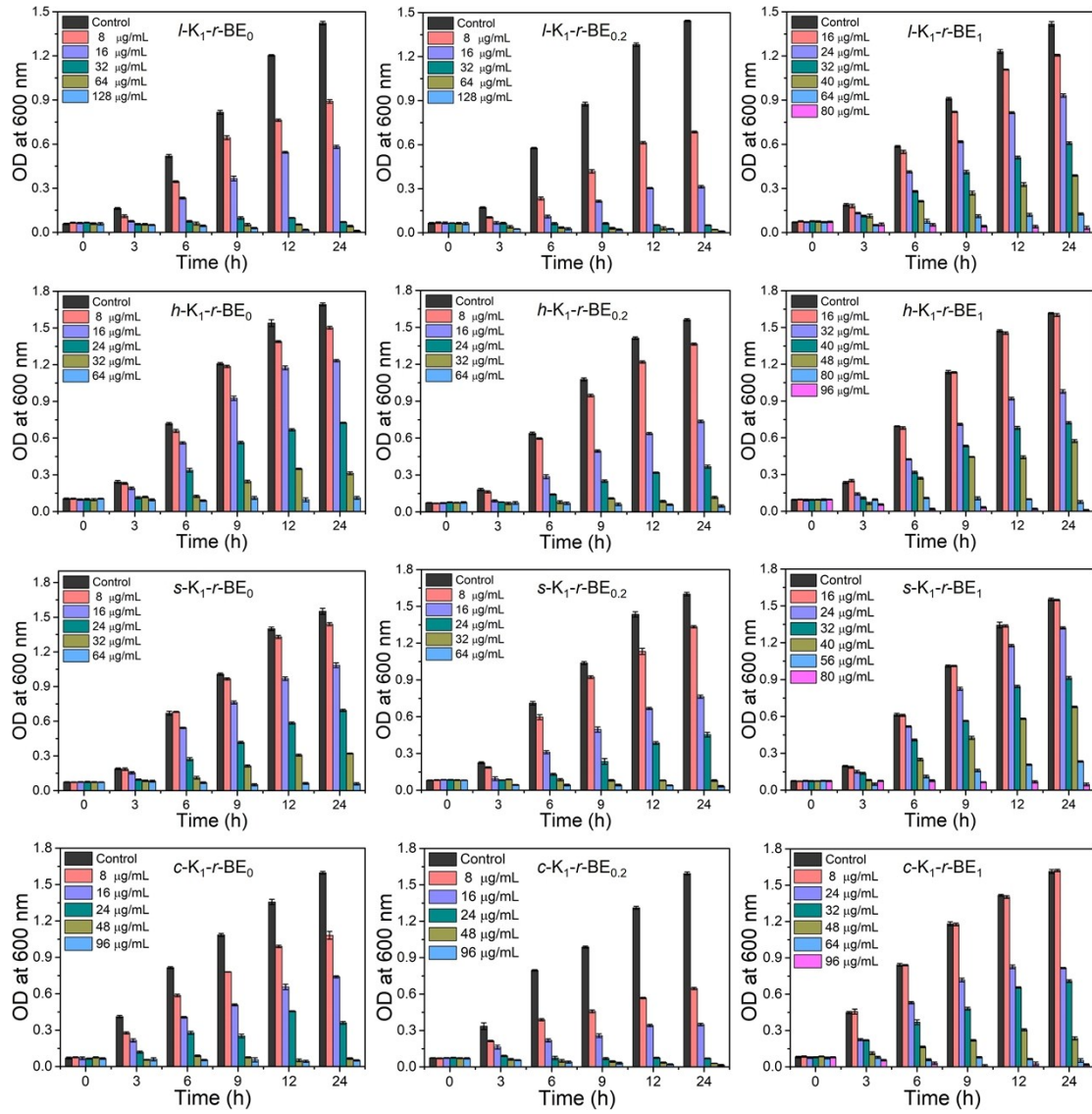


Fig. S11 Dose-dependent growth inhibition curves of *E.coli* in the presence of the TNAPs, respectively.

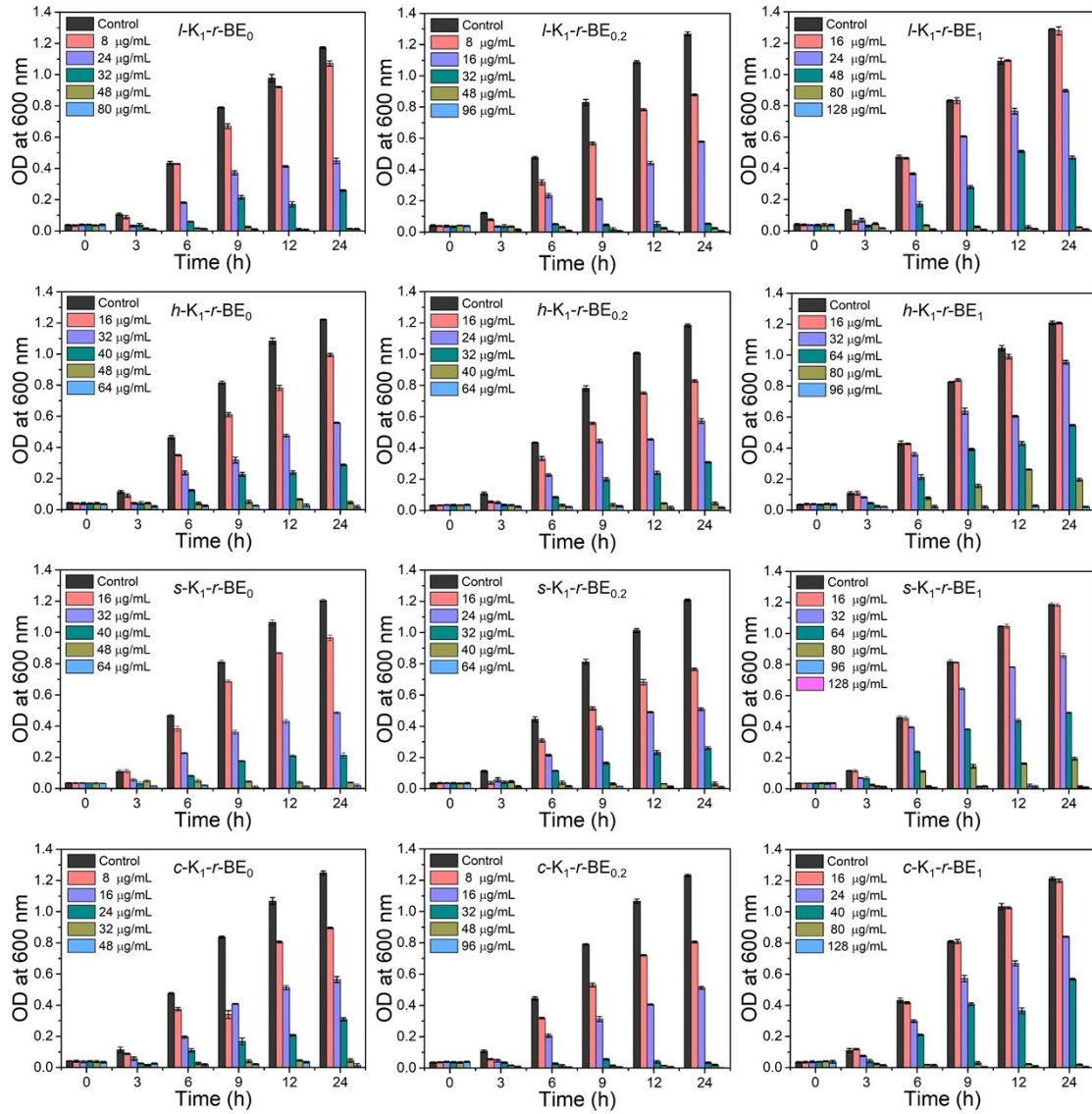


Fig. S12 Dose-dependent growth inhibition curves of *B.subtilis* in the presence of the TNAPs, respectively.

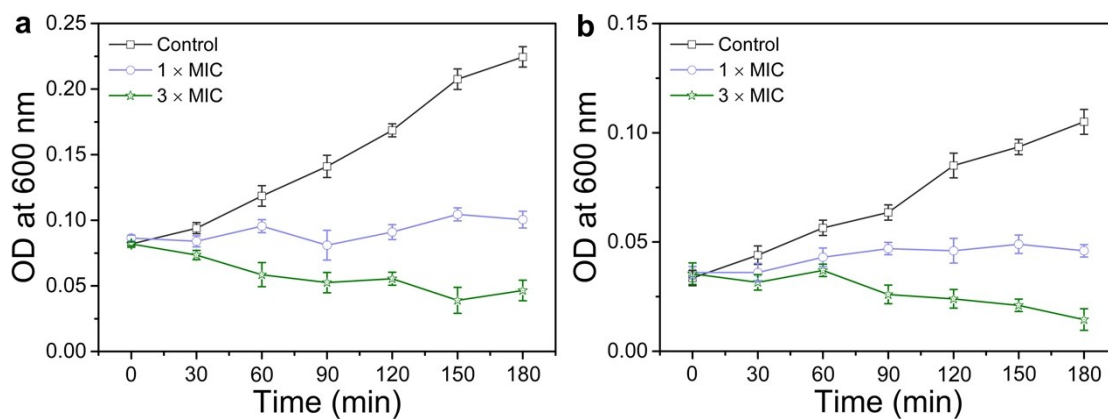


Fig. S13 Growth kinetics of (a) *E. coli* and (b) *B. subtilis* at various concentrations *s-K₁-r-BE_{0.2}*. Bacterial proliferations were observed in both control groups with LB-containing bacteria only. In contrast, upon incubation of bacteria with *s-K₁-r-BE_{0.2}* at 3 × MIC value, it was found that both bacteria were rapidly sedimented to the bottom of the quartz cuvettes within 1 h, leading to the visible decrease of OD value of the supernatant.

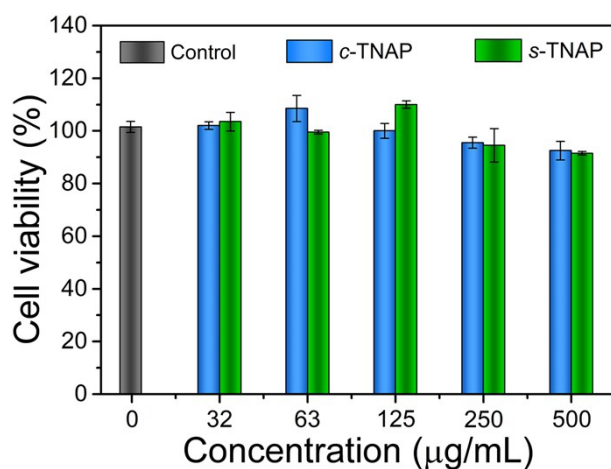


Fig. S14 Cytotoxicity studies of *cyclic-* and *star-*TNAPs against NIH3T3 fibroblast cells.

NMR spectra of synthesized polymers

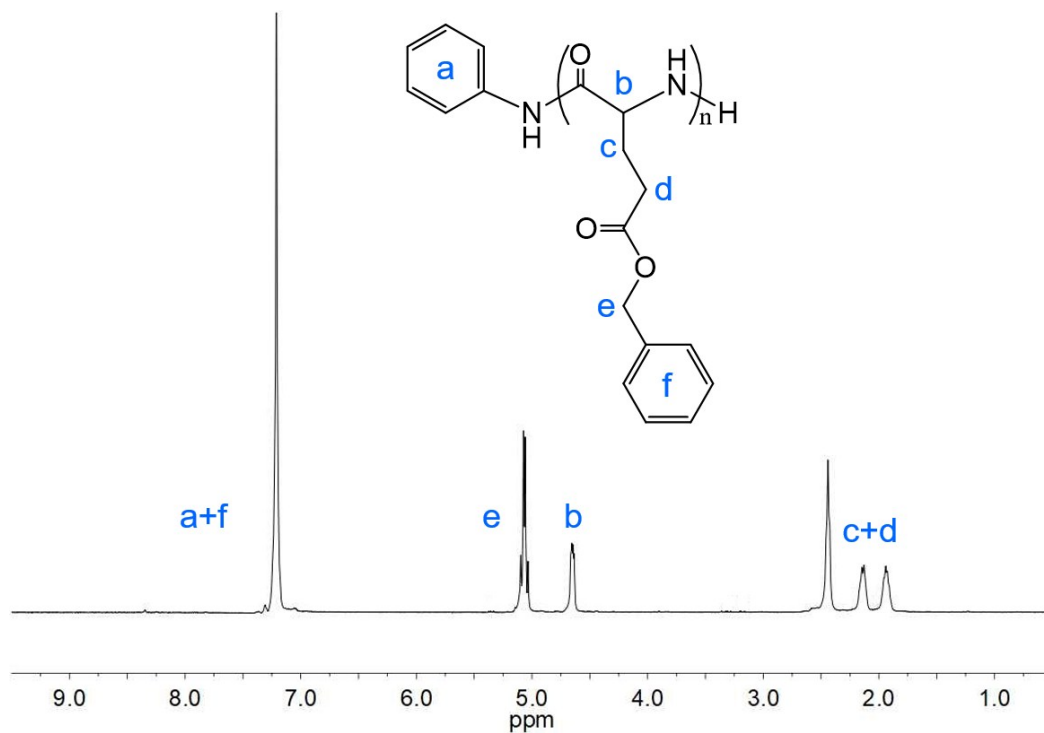


Fig. S15 ^1H NMR spectrum of ANI-initiated *linear* BE in TFA.

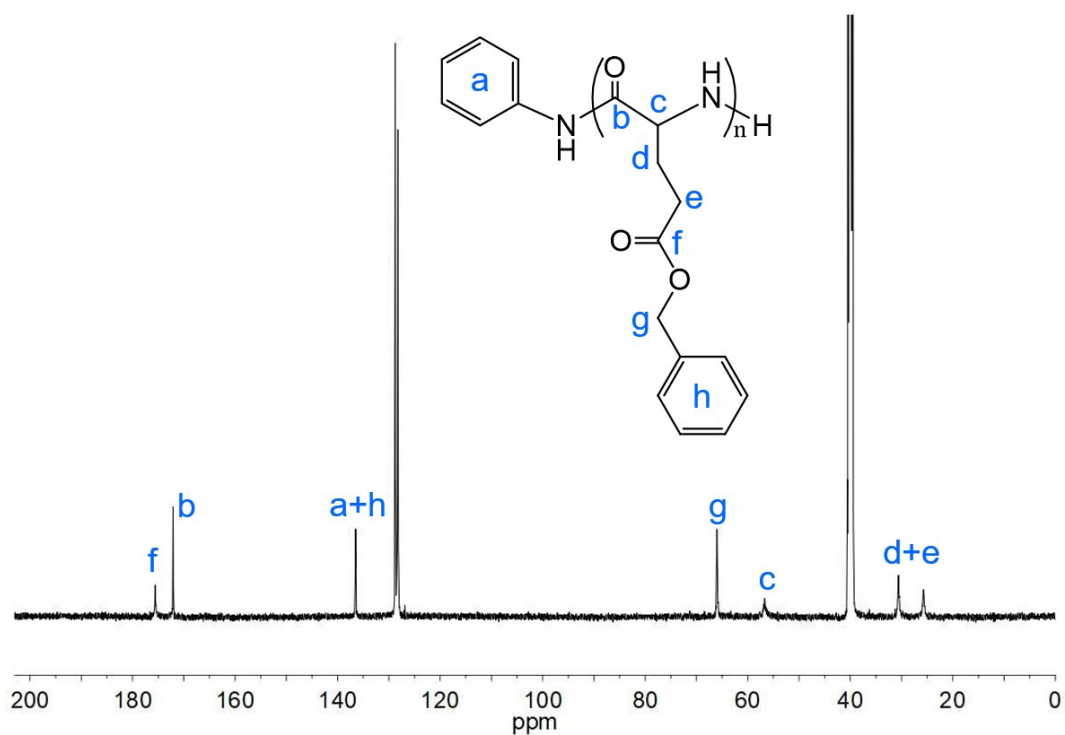


Fig. S16 ^{13}C NMR spectrum of ANI-initiated *linear* BE in $\text{DMSO-}d_6$.

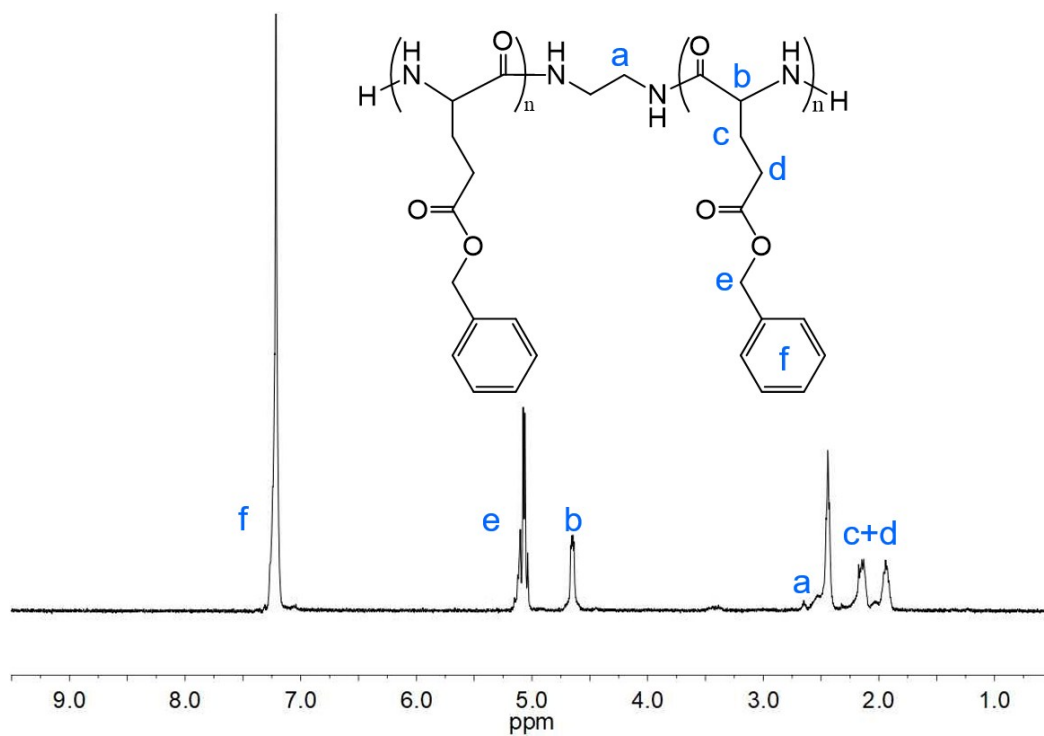


Fig. S17 ^1H NMR spectrum of EDA-initiated *hinged* BE in TFA.

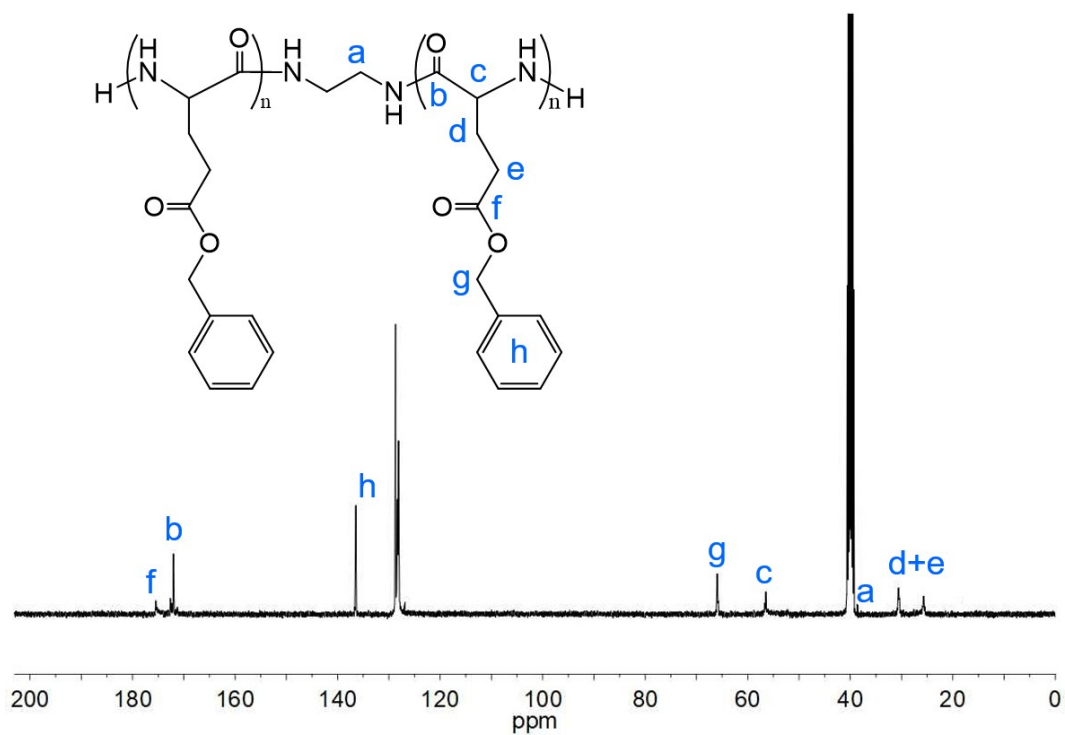


Fig. S18 ^{13}C NMR spectrum of EDA-initiated *hinged* BE in $\text{DMSO-}d_6$.

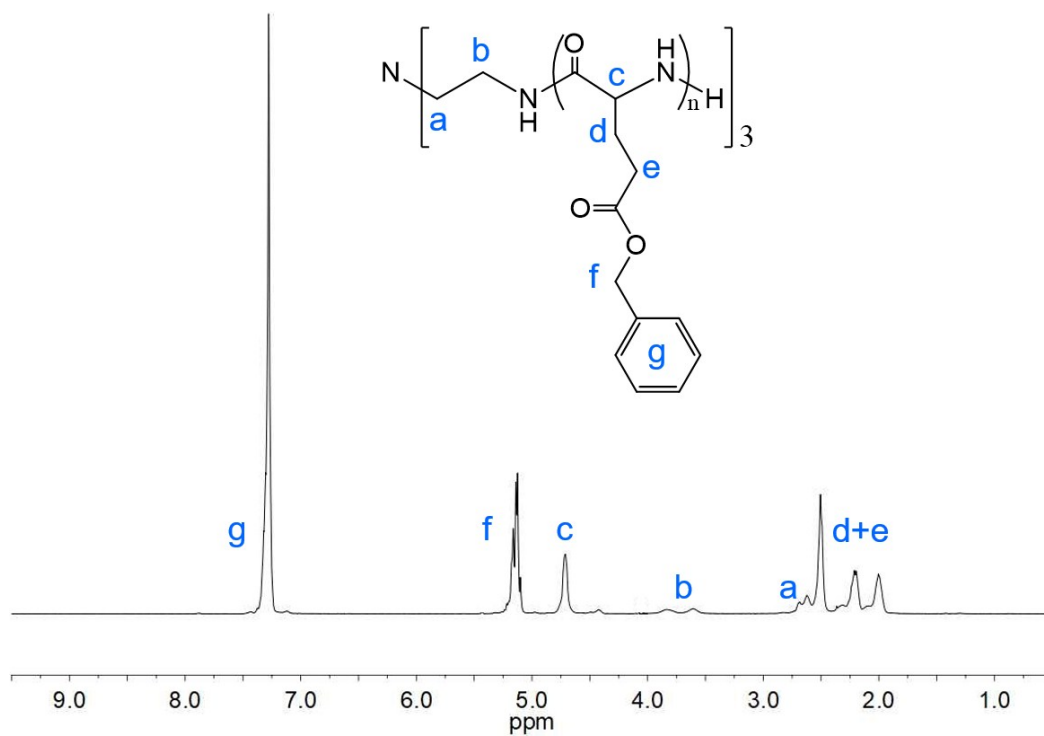


Fig. S19 ^1H NMR spectrum of TREN-initiated *star* BE in TFA.

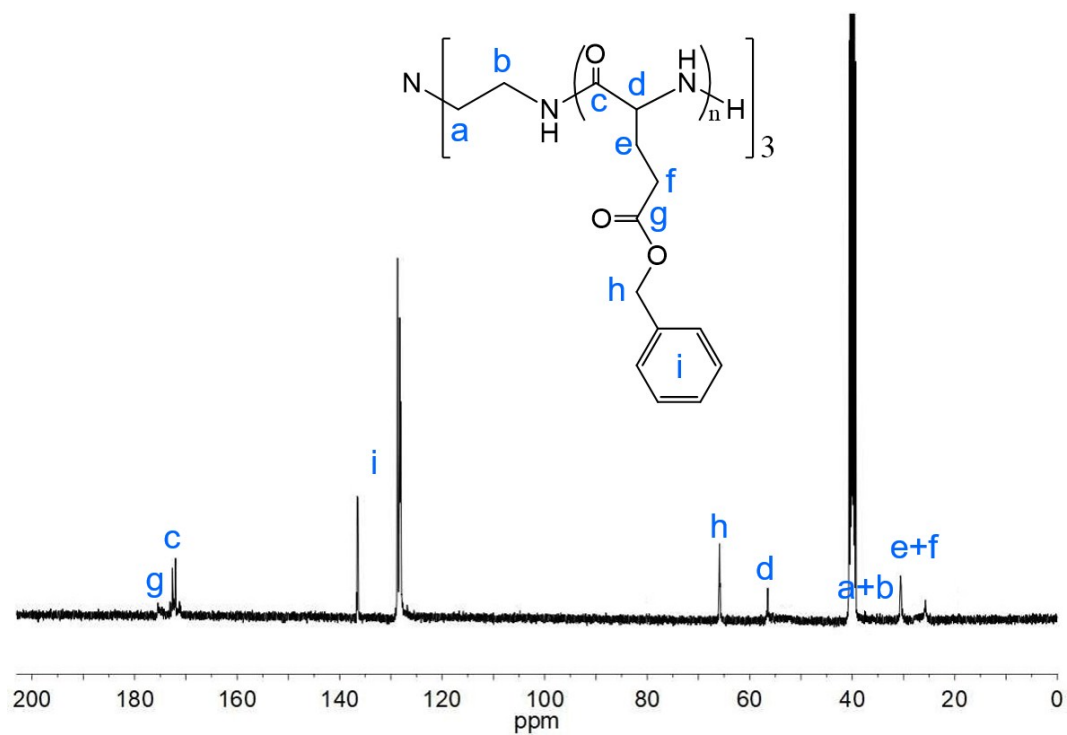


Fig. S20 ^{13}C NMR spectrum of TREN-initiated *star* BE in $\text{DMSO}-d_6$.

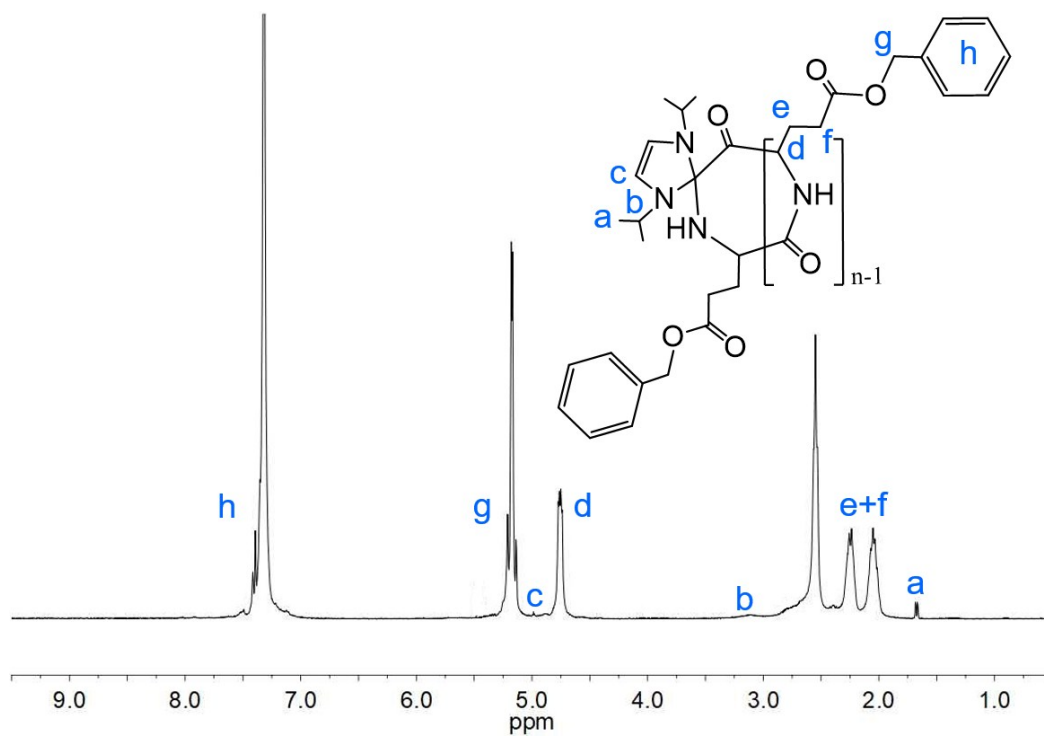


Fig. S21 ^1H NMR spectrum of IHC-initiated *cyclic* BE in TFA.

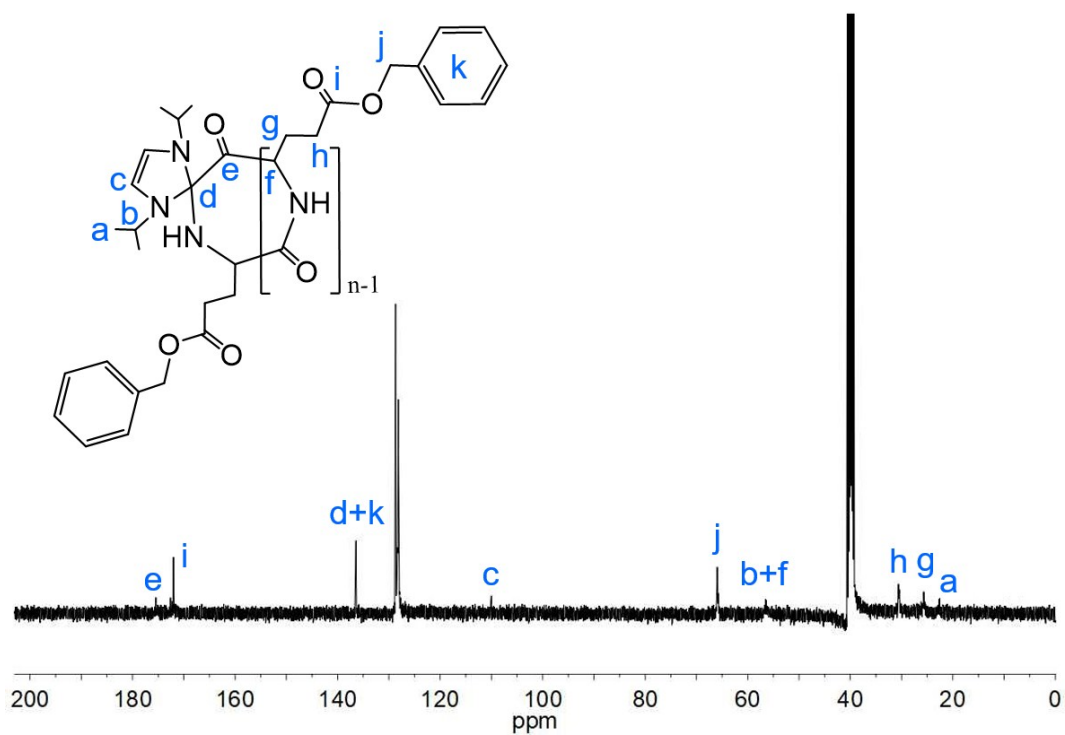


Fig. S22 ^{13}C NMR spectrum of IHC-initiated *cyclic* BE in $\text{DMSO-}d_6$.

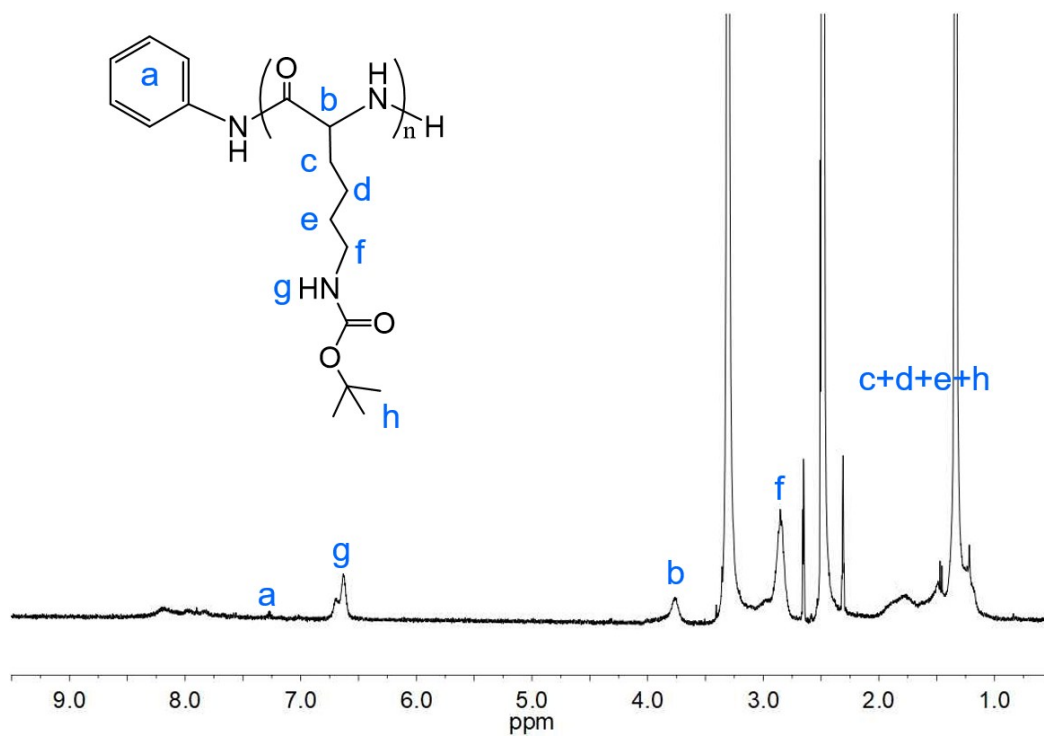


Fig. S23 ^1H NMR spectrum of ANI-initiated *linear* BocK in $\text{DMSO-}d_6$.

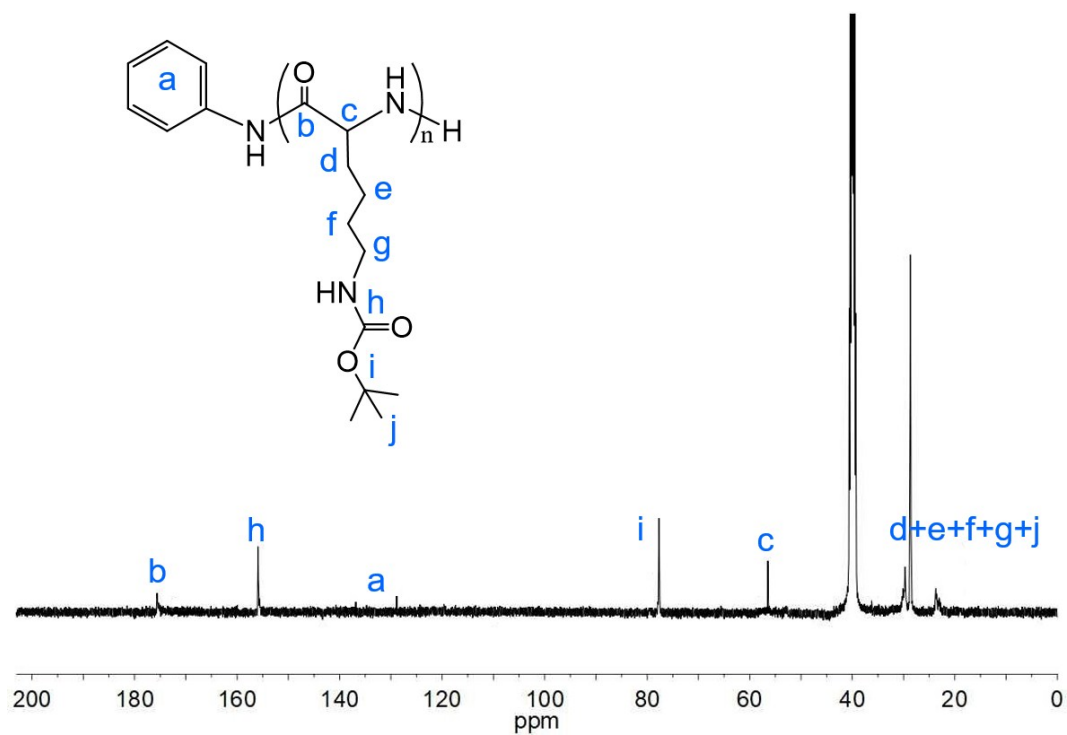


Fig. S24 ^{13}C NMR spectrum of ANI-initiated *linear* BocK in $\text{DMSO-}d_6$.

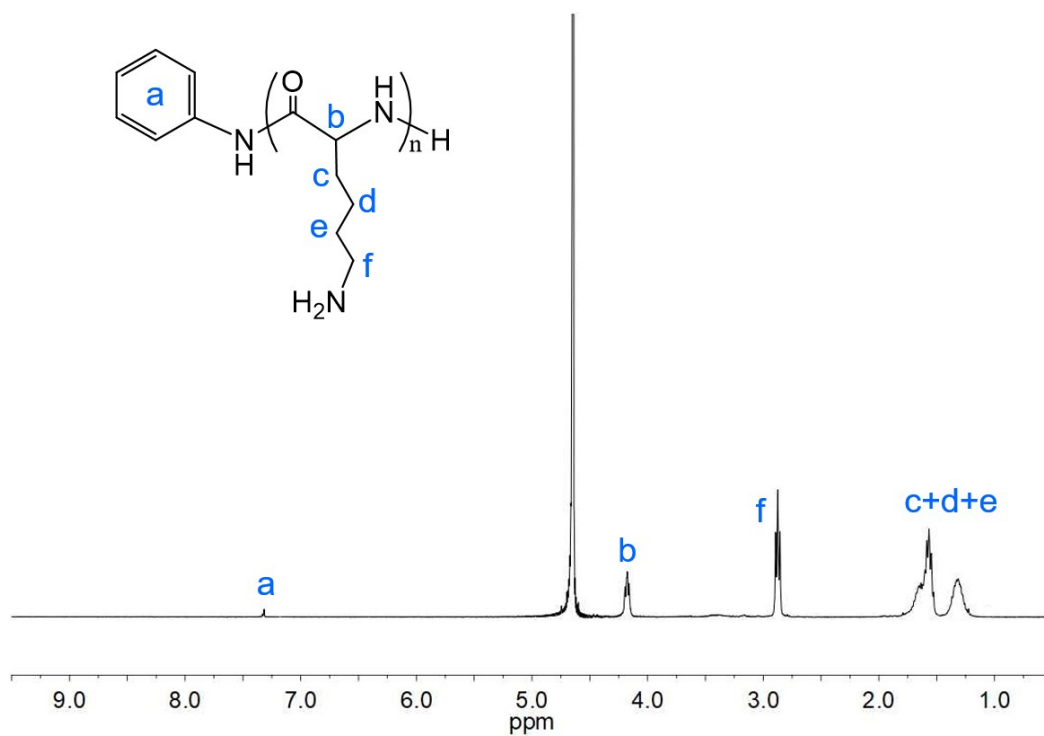


Fig. S25 ¹H NMR spectrum of ANI-initiated *linear* K in D₂O.

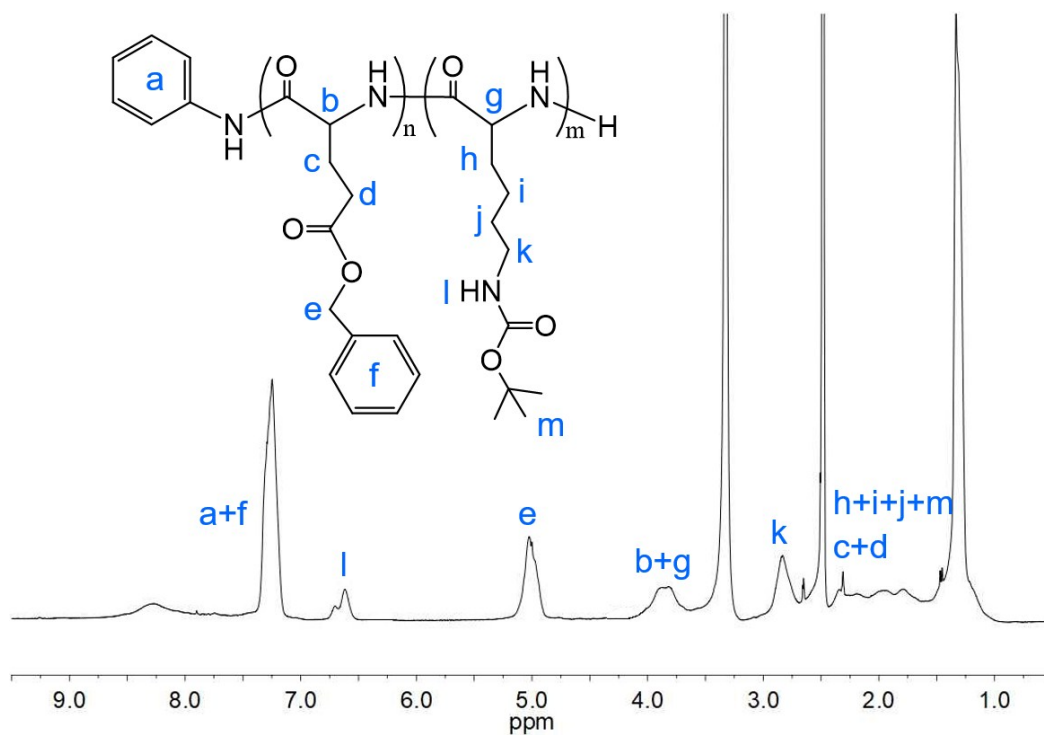


Fig. S26 ¹H NMR spectrum of ANI-initiated *linear* BocK-*r*-BE in DMSO-*d*₆.

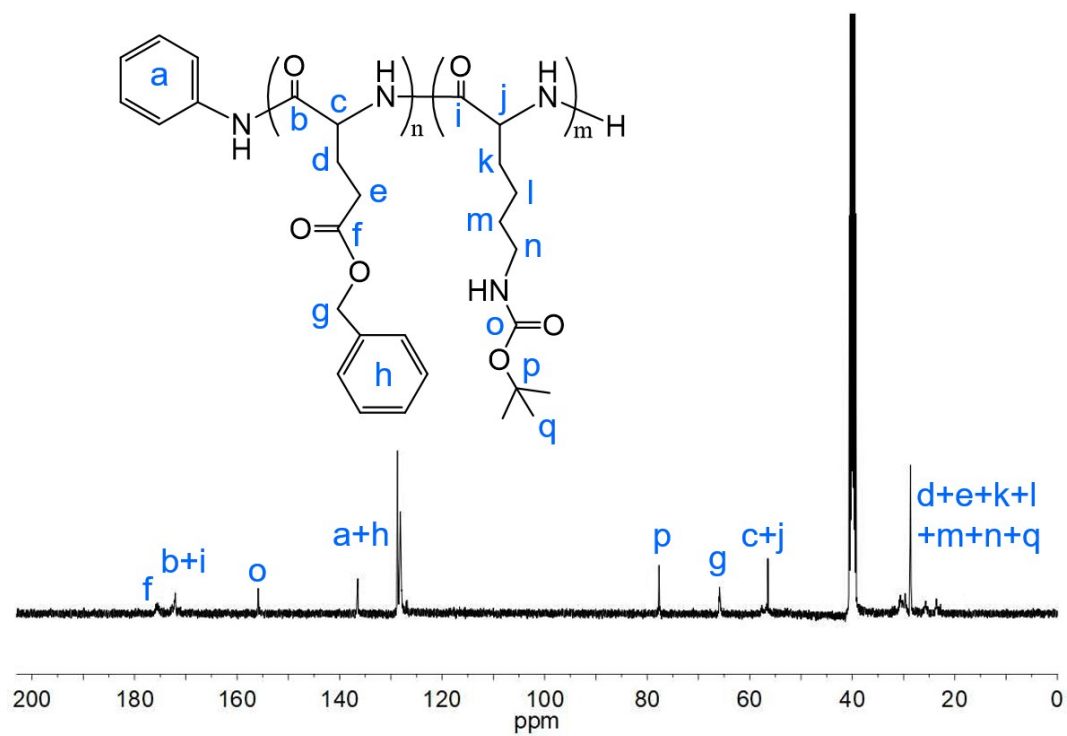


Fig. S27 ^{13}C NMR spectrum of ANI-initiated *linear* BocK-r-BE in $\text{DMSO-}d_6$.

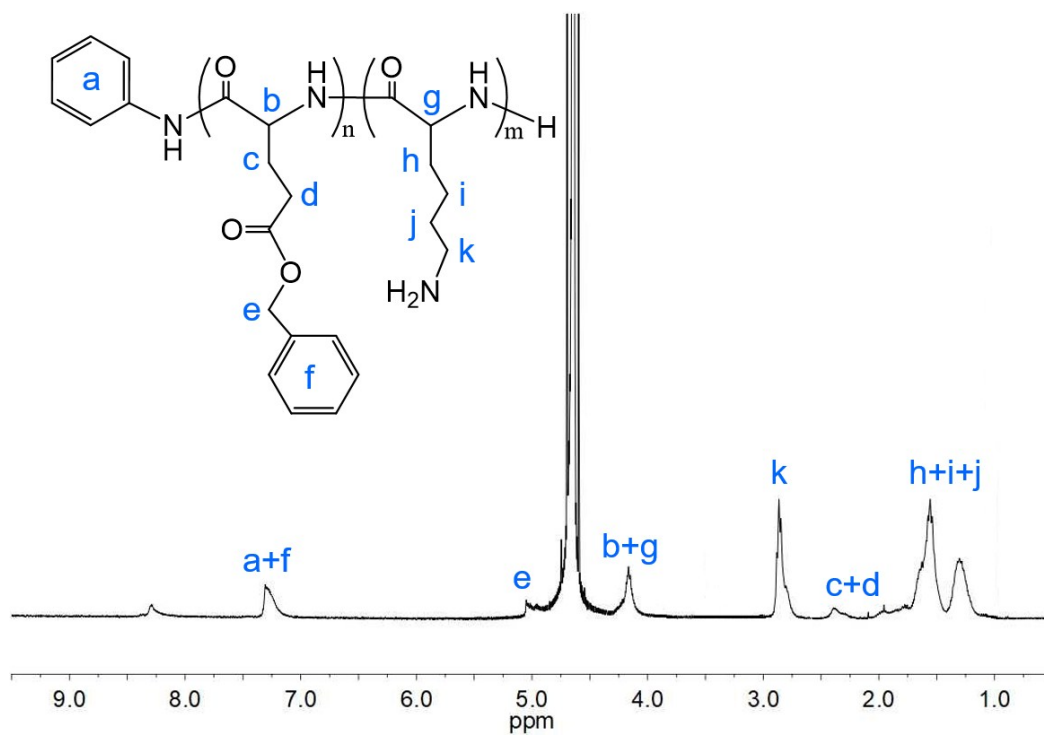


Fig. S28 ^1H NMR spectrum of ANI-initiated *linear* K-r-BE in D_2O .

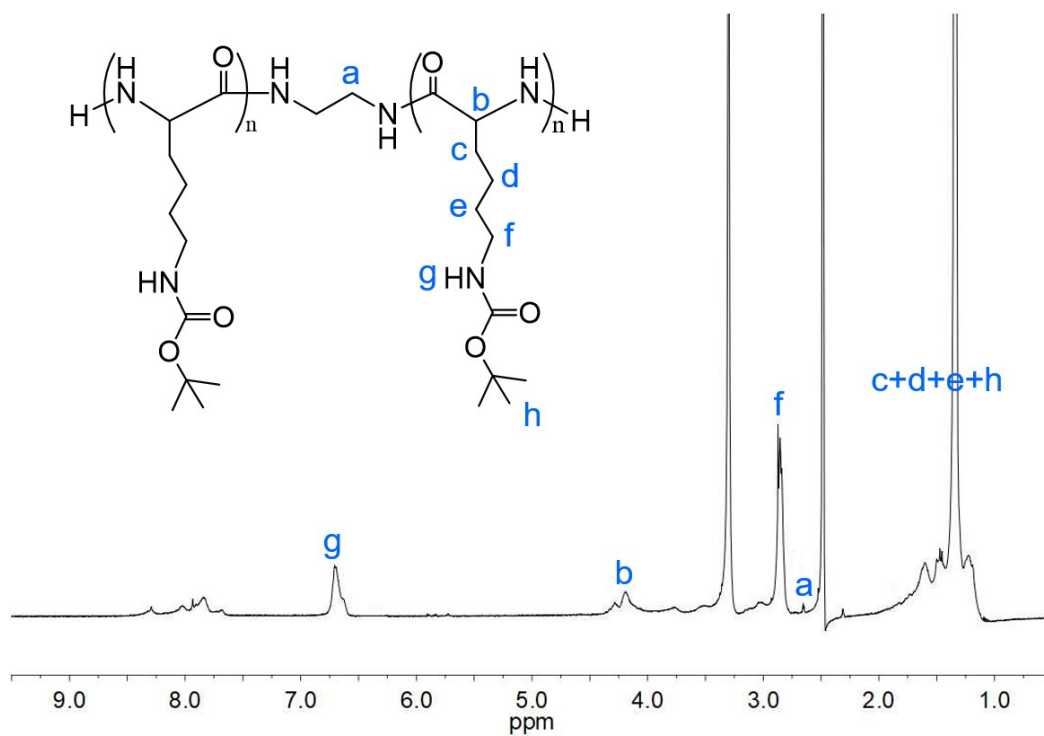


Fig. S29 ^1H NMR spectrum of EDA-initiated *hinged* BocK in $\text{DMSO-}d_6$.

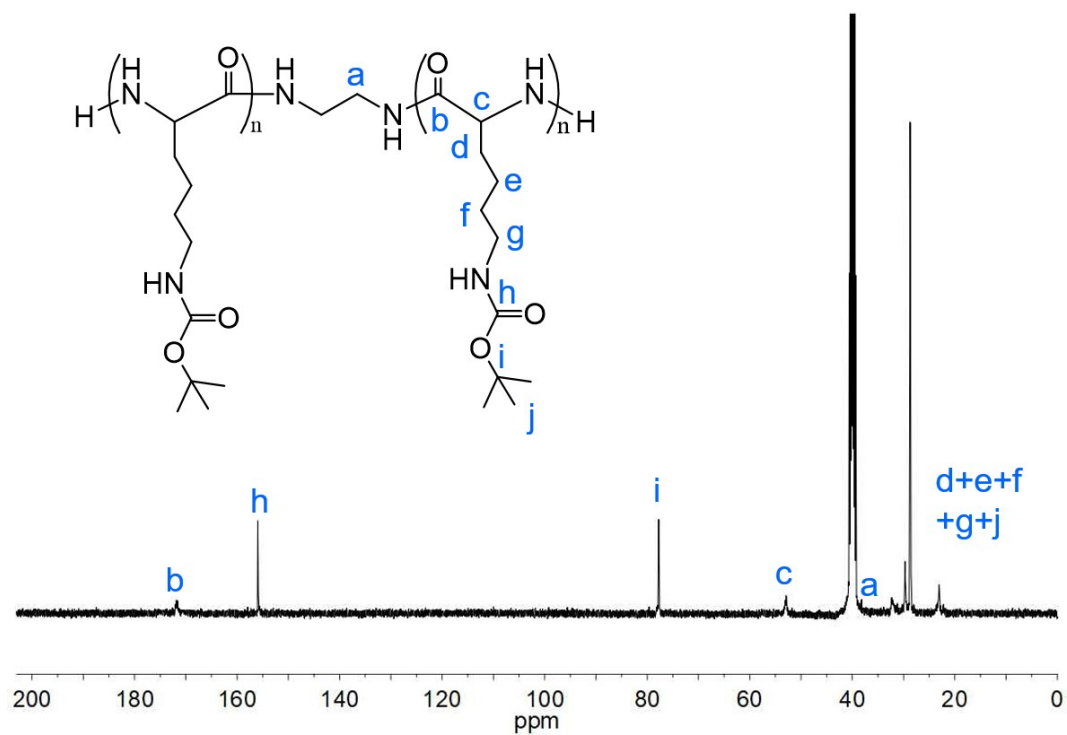


Fig. S30 ^{13}C NMR spectrum of EDA-initiated *hinged* BocK in $\text{DMSO-}d_6$.

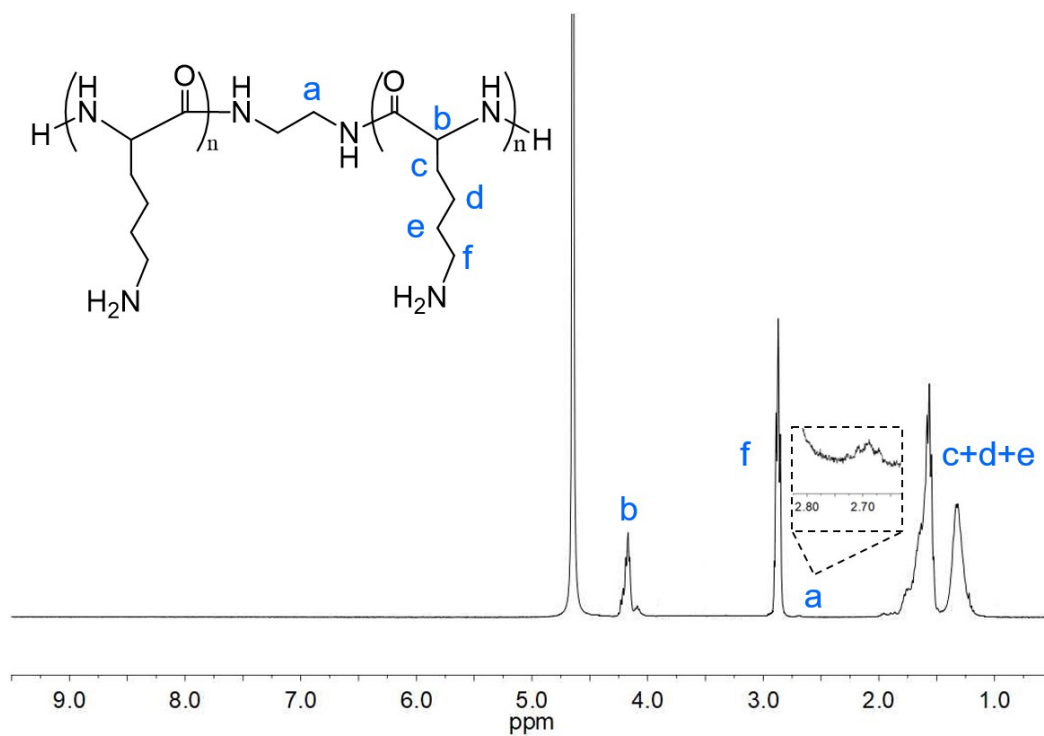


Fig. S31 ^1H NMR spectrum of EDA-initiated *hinged* K in D_2O .

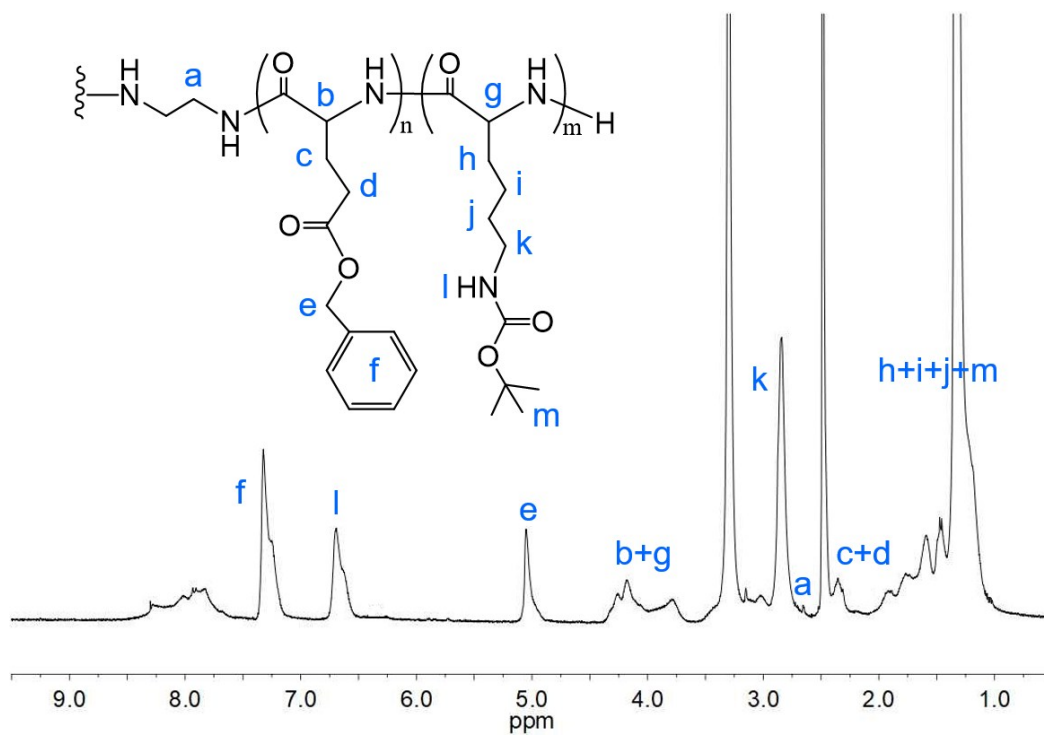


Fig. S32 ^1H NMR spectrum of EDA-initiated *hinged* BocK-r-BE in $\text{DMSO}-d_6$.

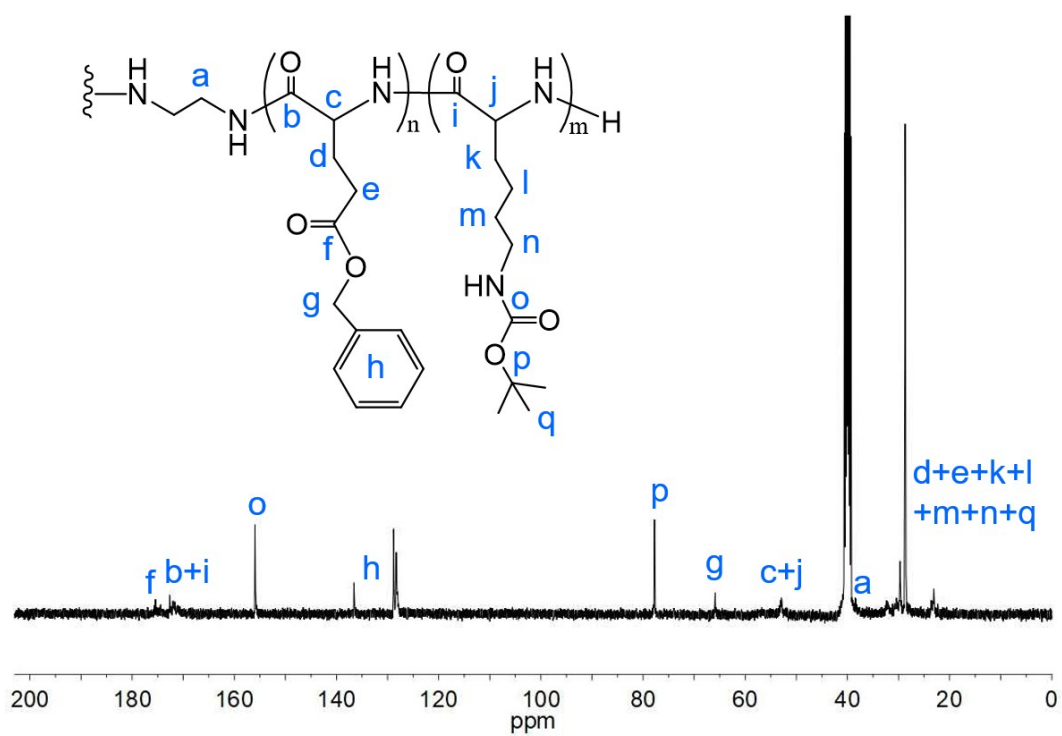


Fig. S33 ^{13}C NMR spectrum of EDA-initiated *hinged* Bock-*r*-BE in $\text{DMSO-}d_6$.

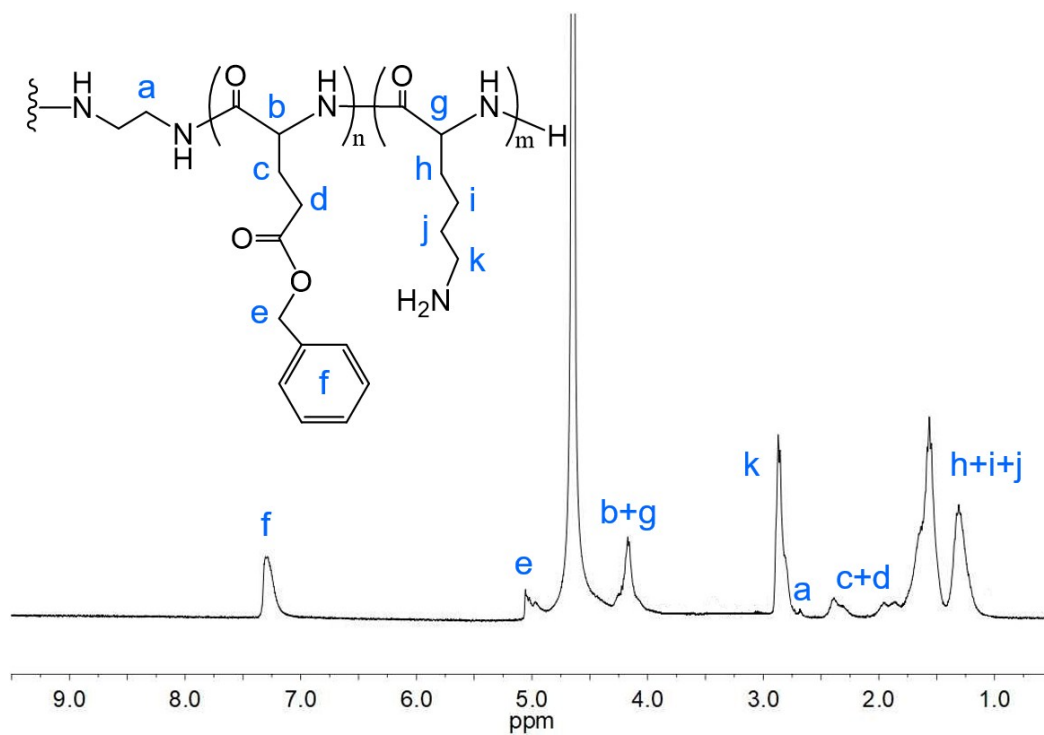


Fig. S34 ^1H NMR spectrum of EDA-initiated *hinged* K-*r*-BE in D_2O .

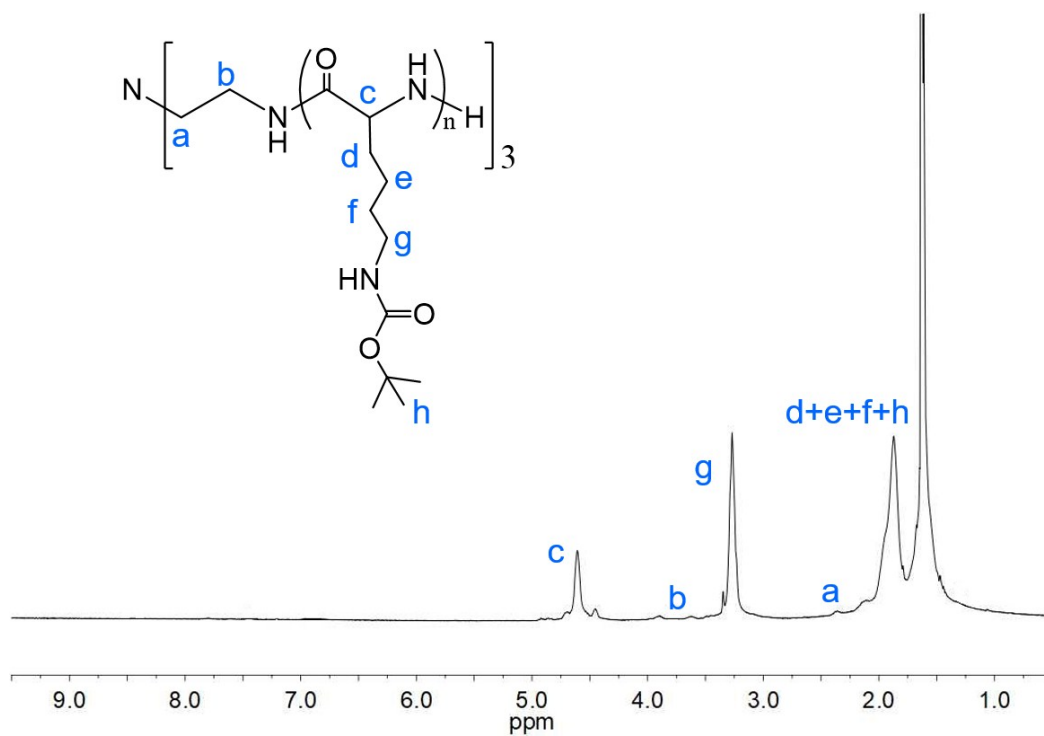


Fig. S35 ^1H NMR spectrum of TREN-initiated *star* BocK in TFA.

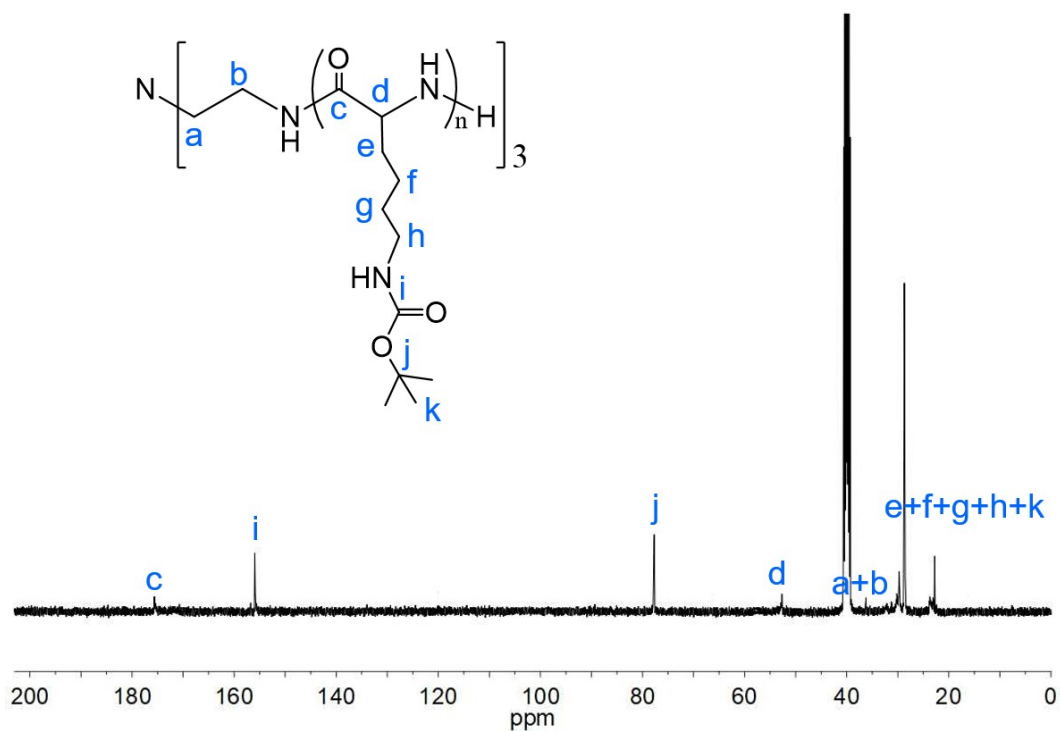


Fig. S36 ^{13}C NMR spectrum of TREN-initiated *star* BocK in $\text{DMSO}-d_6$.

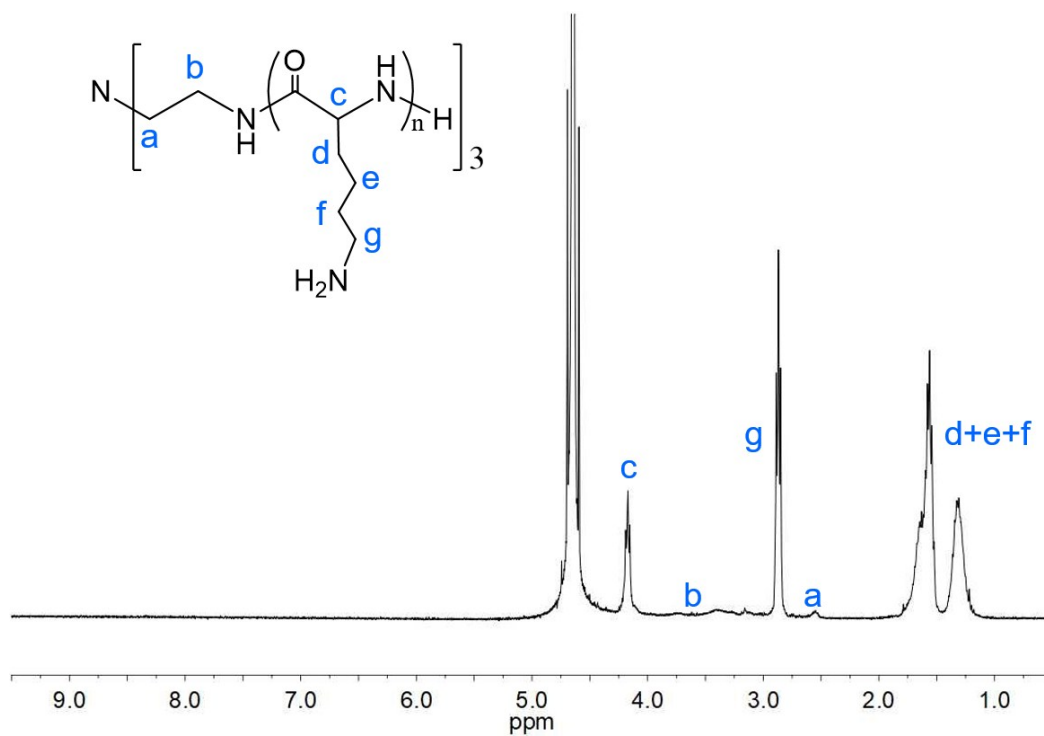


Fig. S37 1H NMR spectrum of TREN-initiated *star* K in D_2O .

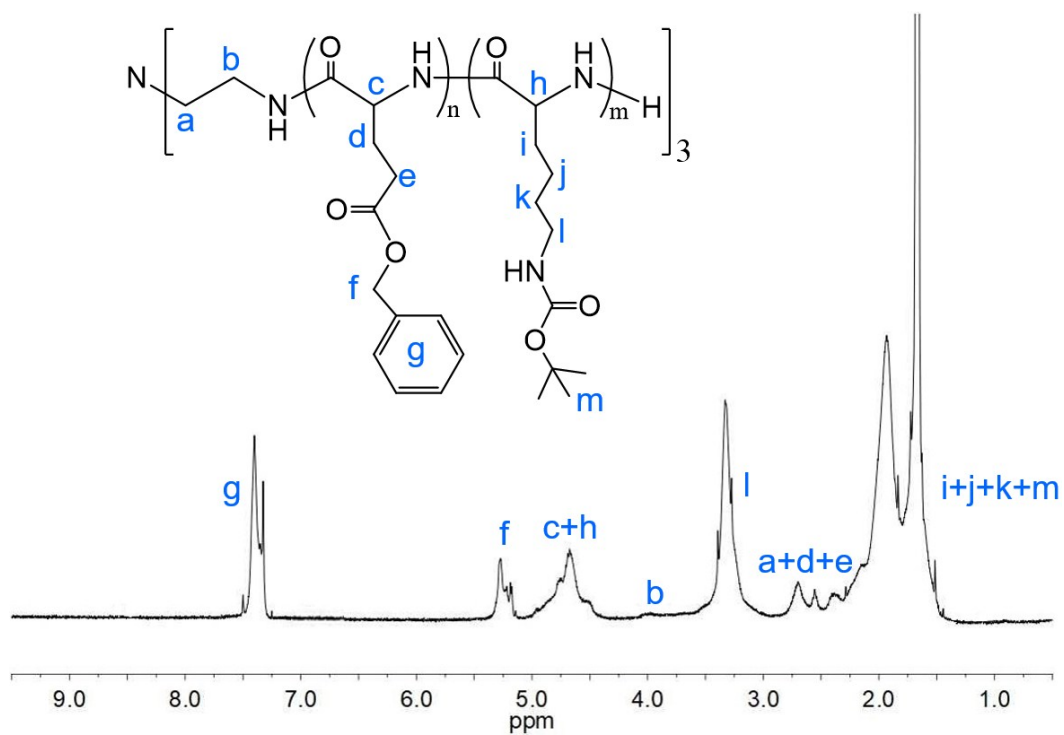


Fig. S38 1H NMR spectrum of TREN-initiated *star* Bock-*r*-BE in TFA.

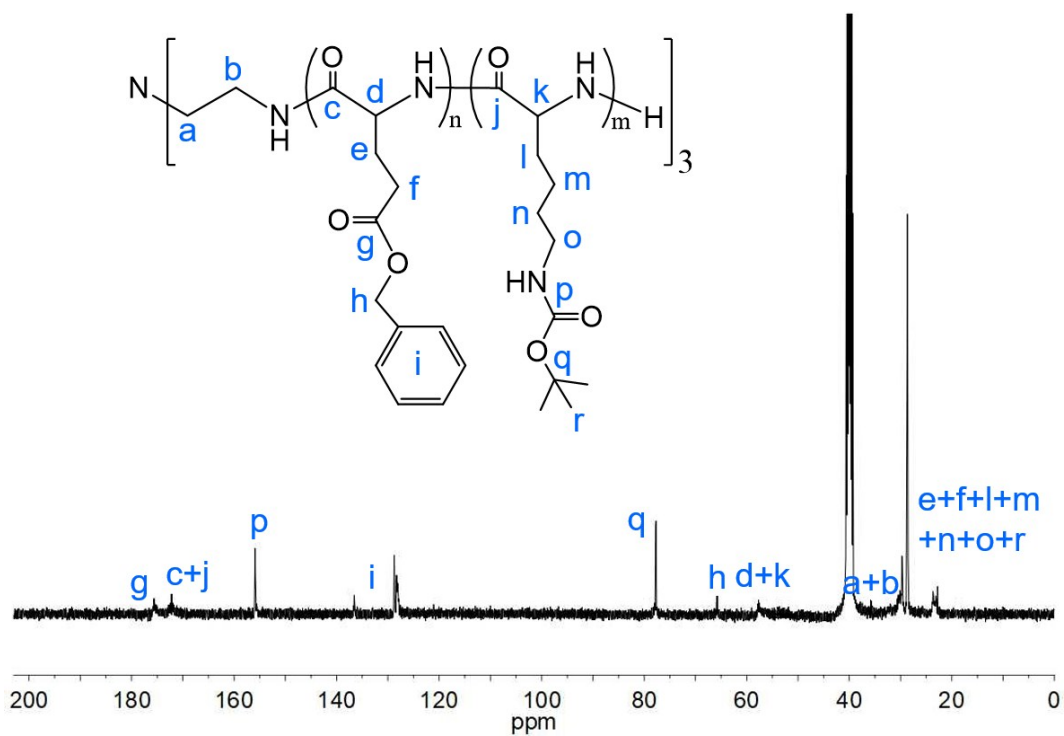


Fig. S39 ^{13}C NMR spectrum of TREN-initiated *star* BocK-*r*-BE in $\text{DMSO-}d_6$.

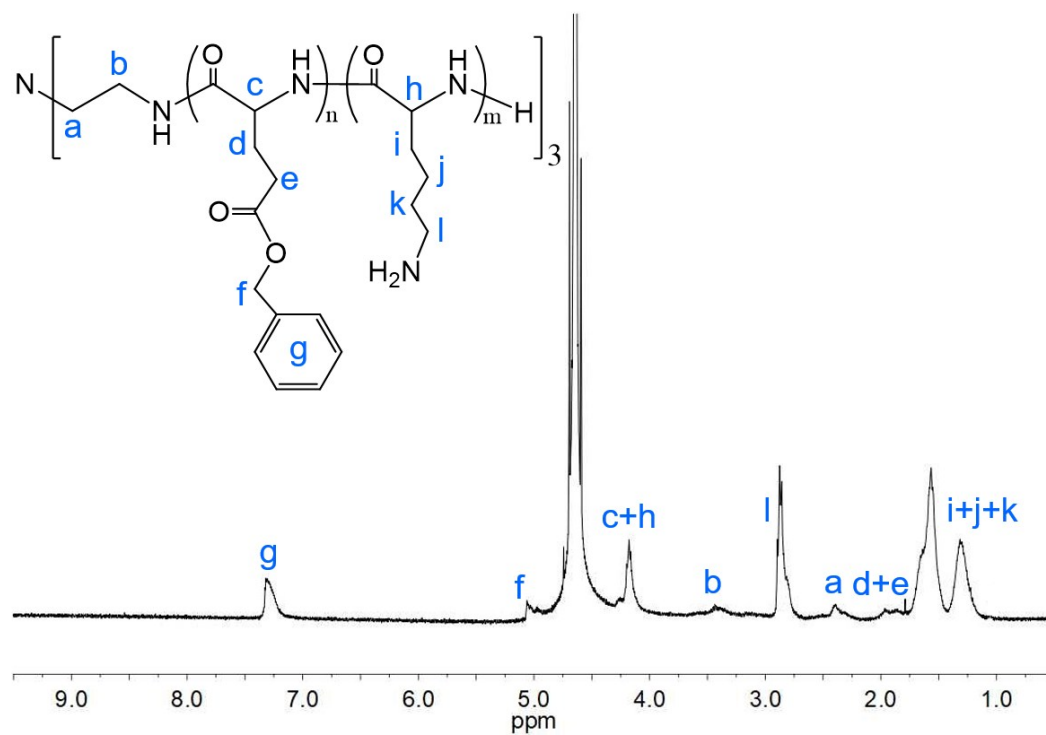


Fig. S40 ^1H NMR spectrum of TREN-initiated *star* K-*r*-BE in D_2O .

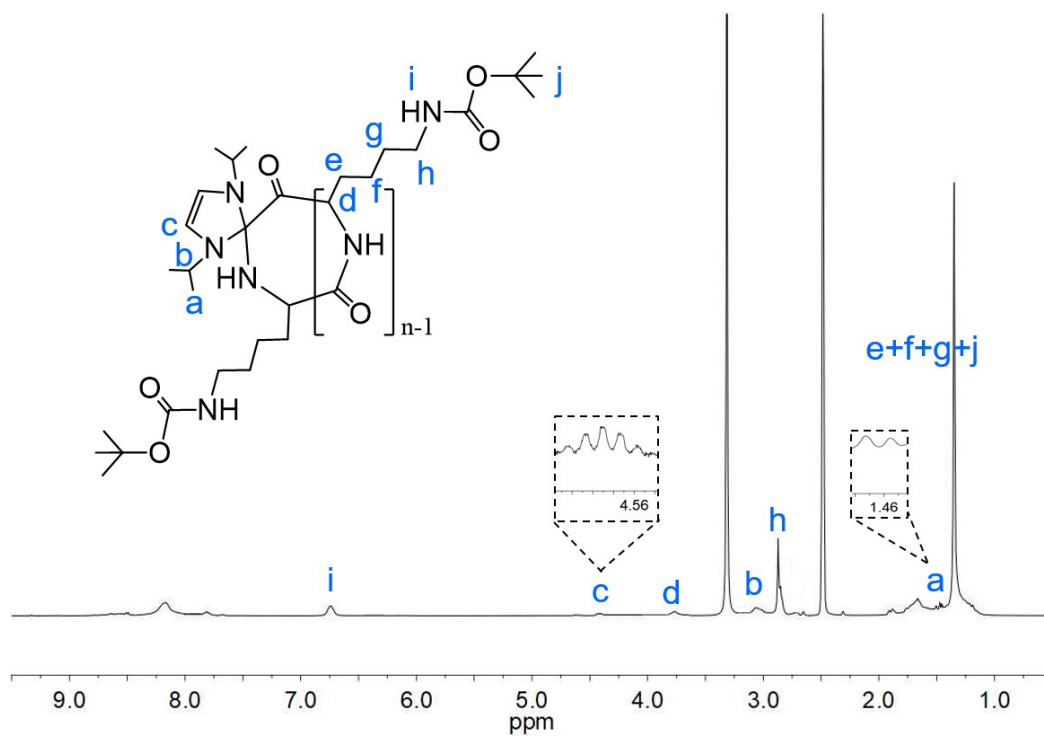


Fig. S41 ^1H NMR spectrum of IHC-initiated *cyclic* BocK in $\text{DMSO-}d_6$.

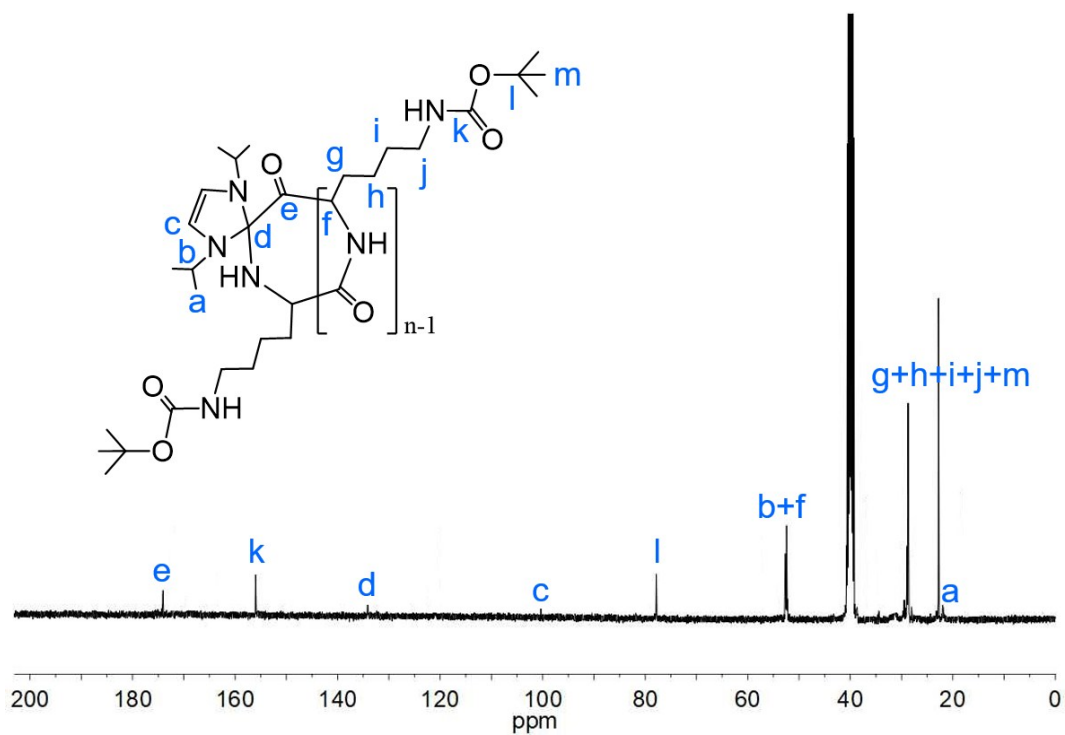


Fig. S42 ^{13}C NMR spectrum of IHC-initiated *cyclic* BocK in $\text{DMSO-}d_6$.

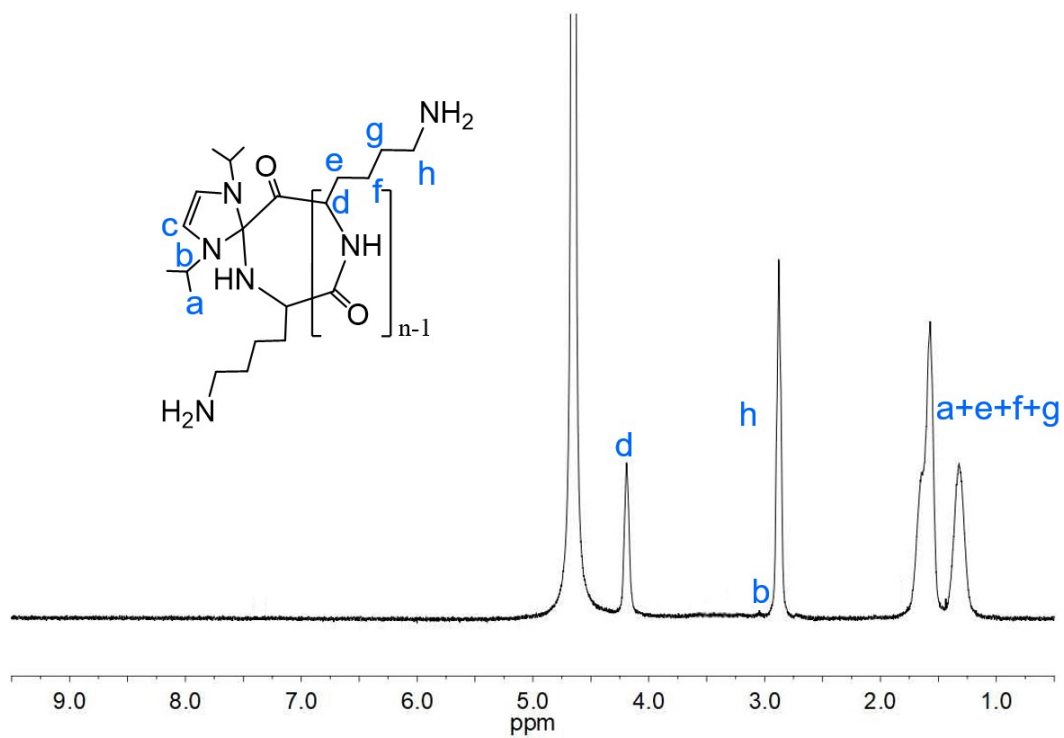


Fig. S43 ^1H NMR spectrum of IHC-initiated *cyclic* K in D_2O .

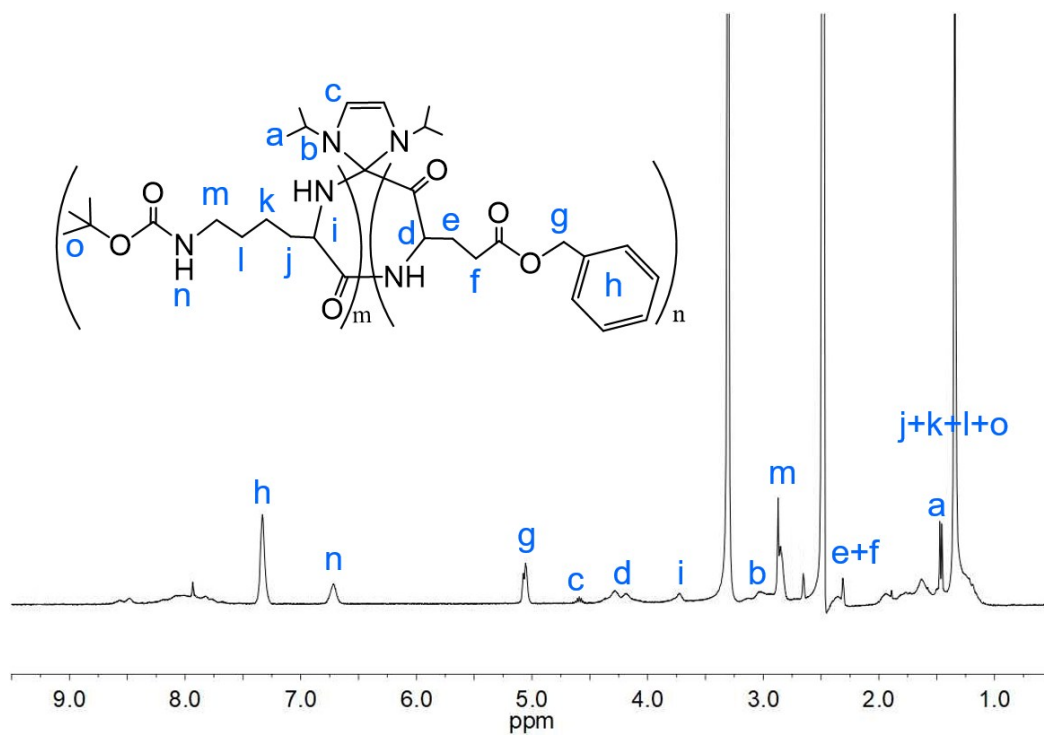


Fig. S44 ^1H NMR spectrum of IHC-initiated *cyclic* Bock-r-BE in $\text{DMSO}-d_6$.

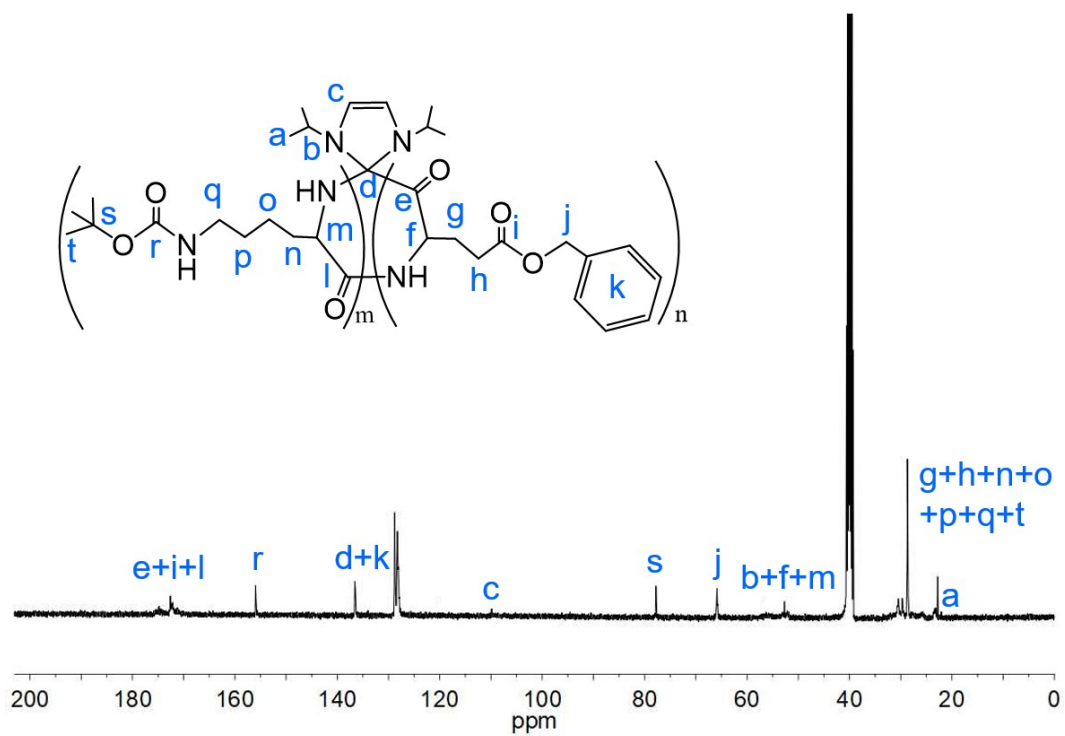


Fig. S45 ^{13}C NMR spectrum of IHC-initiated *cyclic* Bock-*r*-BE in $\text{DMSO-}d_6$.

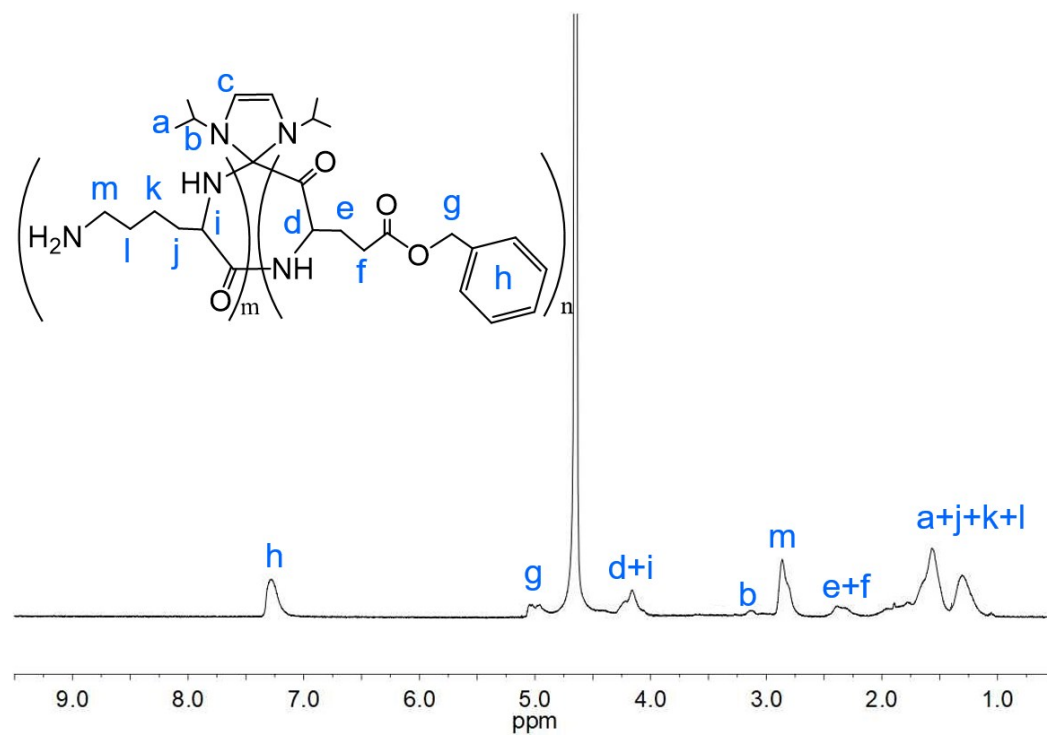


Fig. S46 ^1H NMR spectrum of IHC-initiated *cyclic* K-*r*-BE in D_2O .

3. References

- [S1] M. Fèvre, J. Pinaud, A. Leteneur, Y. Gnanou, J. Vignolle, D. Taton, K. Miqueu and J.-M. Sotiropoulos, *J. Am. Chem. Soc.*, 2012, **134**, 6776–6784.
- [S2] W. H. Daly and D. Poché, *Tetrahedron Lett.*, 1988, **29**, 5859–5862.
- [S3] A. Song, A. A. Rane and K. L. Christman, *Acta Biomater.*, 2012, **8**, 41–50.
- [S4] Y. Wu, D. Zhang, P. Ma, R. Zhou, L. Hua and R. Liu, *Nature Commun.*, 2018, **9**, 5297.
- [S5] T. Stukenkemper, J. F. G. A. Jansen, C. Lavilla, A. A. Dias, D. F. Brougham and A. Heise, *Polym. Chem.*, 2017, **8**, 828–832.
- [S6] W. Zhao, Y. Gnanou and N. Hadjichristidis, *Biomacromolecules*, 2015, **16**, 1352–1357.
- [S7] J. Zou, J. Fan, X. He, S. Zhang, H. Wang and K. L. Wooley, *Macromolecules*, 2013, **46**, 4223–4226.
- [S8] P. Hui, J. Ling and Z. Shen, *J. Polym. Sci., Part A: Polym. Chem.* 2012, **50**, 1076–1085.
- [S9] L. Hua and J. Cheng, *J. Am. Chem. Soc.*, 2007, **46**, 14114–14115.
- [S10] H. R. Kricheldorf, C. Von Lossow and G. Schwarz, *J. Polym. Sci., Part A: Polym. Chem.* 2006, **44**, 4680–4695.
- [S11] H. R. Kricheldorf, C. Von Lossow and G. Schwarz, *J. Polym. Sci., Part A: Polym. Chem.* 2005, **43**, 5690–5698.
- [S12] T. J. Deming, *Nature*, 1997, **390**, 386–389.
- [S13] D. Pranantyo, L.-Q. Xu, Z. Hou, E.-T. Kang and M. B. Chan-Park, *Polym. Chem.*, 2017, **8**, 3364–3373.
- [S14] Y. Hong, Y. Xi, J. Zhang, D. Wang, H. Zhang, N. Yan, S. He and J. Du, *J. Mater. Chem. B.*, 2018, **6**, 6311–6321.
- [S15] N. Rodrigues de Almeida, Y. Han, J. Perez, S. Kirkpatrick, Y. Wang and M. C. Sheridan, *ACS Appl. Mater. Interfaces*, 2019, **11**, 2790–2801.
- [S16] X. Zhou, J. He and C. Zhou, *Polym. Chem.*, 2019, **10**, 945–953.
- [S17] Y. Xi, T. Song, S. Tang, N. Wang and J. Du, *Biomacromolecules*, 2016, **17**,

3922–3930.

[S18] S. J. Shirbin, I. Insua, J. A. Holden, J. C. Lenzo, E. C. Reynolds, N. M. O'Brien-Simpson and G. G. Qiao, *Adv. Healthc. Mater.*, 2018, **7**, 1800627.

[S19] C. Zhou, Y. Yuan, P. Zhou, F. Wang, Y. Hong, N. Wang, S. Xu and J. Du, *Biomacromolecules*, 2017, **18**, 4154–4162.

[S20] V. S. Fluxà, N. Maillard, M. G. P. Page and J.-L. Reymond, *Chem. Commun.*, 2011, **47**, 1434–1436.